SPECTROELECTROCHEMICAL STUDIES OF ADSORBED As(III) AND As(V) ON FERRIHYDRITE

A Thesis Submitted to the College of

Graduate Studies and Research

In Partial Fulfillment of the Requirements

For the Degree of Masters of Science

In the Department of Chemistry

University of Saskatchewan

Saskatoon

By

JESSICA ANN SIGRIST

Permission to Use

In presenting this thesis in partial fulfilment of the requirements for a Postgraduate degree from the University of Saskatchewan, I agree that the Libraries of this University may make it freely available for inspection. I further agree that permission for copying of this thesis in any manner, in whole or in part, for scholarly purposes may be granted by the professor or professors who supervised my thesis work or, in their absence, by the Head of the Department or the Dean of the College in which my thesis work was done. It is understood that any copying or publication or use of this thesis or parts thereof for financial gain shall not be allowed without my written permission. It is also understood that due recognition shall be given to me and the University of Saskatchewan in any scholarly use which may be made of any material in my thesis.

Requests for permission to copy or to make other use of material in this thesis in whole or part should be addressed to:

Head of the Department of Chemistry

University of Saskatchewan

Saskatoon, Saskatchewan, S7N 5C9

Canada

Abstract

At Cameco mine sites in northern Saskatchewan, naturally occurring elements of concern (EOC) such as As, Ni, Mo, and Se are present in uranium ore bodies. Ferrihydrite (Fh) is found in tailings management facilities (TMF) and is known to sequester arsenates and arsenites. Fh is known to be metastable and undergo phase transformations to goethite (α-FeOOH) and hematite (α-Fe_2O_3). Reductive conditions are known to be a driving force in Fh transformation and the release of adsorbed As species from the surface. This study uses electrochemistry to control reductive potentials applied to Fh adsorbed As species. Electrochemistry was coupled with attenuated total reflectance Fourier transform infrared (ATR-FTIR) spectroscopy to determine the behaviour of adsorbed arsenate and arsenite on the Fh surface. The potentials required to desorb As(III) and As(V) from the Fh surface were negative enough to cause the reduction of water, thus increasing the pH of the solution through the generation of OH^-. In order to measure the extent of the pH change a miniature palladium/palladium oxide pH sensor was fabricated in order to make *in-situ* pH measurements during spectroelectrochemical studies. Additionally, *in-situ* solution potential (Eh) measurements were made during potential control. It was found that potential induced pH and Eh changes were significant enough to release arsenite from the Fh surface. Arsenate was also found to desorb from Fh during the application of reductive potentials though successive deprotonation leading to a totally deprotonated As(V) species.

Acknowledgments

First and foremost I would like to thank my supervisor Dr. Ian Burgess for his support over the last couple years, his patience and understanding ultimately got me to this point.

I would also like to thank the groups that made their facilities available to me. Thanks to Dr. Jim Hendry's group, specifically Dr. Mario Gomez for help with the synthesis of ferrihydrite. I would like to thank Dr. Andrew Grosvenor for allowing me to use his furnaces. John thanks for your help with this even when it turned into more than just one wire. I would like to thank Ted and Blair in the Physics Machine Shop who helped me along the way with various requests but specifically, with the fabrication of the spectroelectrochemical cell. Without their help I would not have been able to perform any of these experiments. I would like to thank the researchers at the Cameco research facility for performing XRD and Raman analysis when needed in addition to the helpful comments throughout this project.

To all my friends and family who always were interested in hearing about my project. I appreciate the support you have given me during the last two years. Thank-you to the past and present Burgess group members and fellow students within the Department for support throughout this work.

Lastly, I would like to thank Ryan who has supported me through this from day one. Thanks for encouraging me to go back to school and supporting me throughout this entire process. I appreciate that you were always just as excited as I was about various aspects of my project. Your confidence in me over the last several years has helped me through this process.

To my husband

Thank-you for your love and support along the way

Table of Contents

List of Figures

List of Tables

List of Abbreviations

AOI	angle of incidence
ATR-FTIR	attenuated total reflectance Fourier transform infrared
ATR-SEIRAS	attenuated total reflectance surface enhanced infrared absorption spectroscopy
CE	counter electrode
CV	cyclic voltammetry
EOC	elements of concern
EXAFS	extended X-ray absorption fine structure
Fh	ferrihydrite
IRE	internal reflection element
M	molar
mV	millivolts
OCC	open circuit conditions
OCP	open circuit potential
pXRD	powder X-ray diffraction
RE	reference electrode
SCE	saturated calomel electrode
TMF	tailings management facility
WE	working electrode
α-FeOOH	goethite
α-Fe_2O_3	hematite

1. Introduction and Literature Review

1.1. Thesis Overview

The effluent from the uranium milling processes in northern Saskatchewan is stored in tailings management facilities (TMFs). It is of great importance to have an understanding of the long-term behaviour of the mobility and sequestration of elements of concern (EOC), such as arsenic, nickel, selenium, and molybdenum in the TMFs. Due to its toxicity many studies have investigated the fate of arsenate, As(V), and arsenite, As(III), in TMFs. The sequestration of As(V) and As(III) is known to occur through their adsorption on iron(III) (oxy)hydroxides, specifically ferrihydrite (Fh). Ferrihydrite is known to be metastable and undergoes a phase transformation to more thermodynamically stable crystalline forms such as goethite (α-FeOOH) and hematite (α-Fe_2O_3). It is understood that under reductive conditions Fh undergoes phase transformation in addition to the release of adsorbed species.[1-4] The solution potential (Eh) and pH have a large influence on the species in solution and their adsorption on mineral phases. In TMFs, the solution potential is influenced by many complicated and interconnecting factors; potential determining ions, concentration of dissolved O_2, pH, and redox pinning bacteria. Modeling the fate of EOC adsorption requires fundamental knowledge of the influences of redox conditions. Current methods for controlling the Eh in laboratory simulated TMF conditions use reducing bacteria or potential determining ions.[5-7] These methods are applicable although they introduce competing factors and limit one's ability to directly correlate the Eh to the fate of EOCs such as As(V) and As(III). The use of electrochemistry for applying and controlling reductive conditions appears to be an appealing method to reduce competing factors. The conjunction of electrochemistry and attenuated total reflectance Fourier transform infrared (ATR-FTIR) spectroscopy to perform *in-situ* experiments

leads to the possibility of associating specific reductive conditions to the fate of adsorbed As(III) and As(V) on the Fh surface.

1.2. Cameco Tailings Facilities

One of the world's largest and highest-grade uranium ore bodies is located in the Athabasca Basin of northern Saskatchewan, roughly 650 km north of Saskatoon. Cameco has several mining operations located in this area which use pit tailings management facilities. Over the years these TMFs have evolved to adapt to increased regulations, and increased production. First generation tailings facilities made use of low or natural lakes, while second generation facilities were engineered TMFs above the water table.[8] Uranium mining in this area is completed by mining in open pits. The development of third generation TMFs made use of these open pits for the use of tailings storage below the water table, which limits the possibility of contaminants in the tailings reaching the ground water supply.[8] The in-pit TMF located at the Rabbit Lake facility measures 425 m long x 300 m wide x 91 m deep and is lined with a permeable layer of sand to allow for the movement of water.[9] The ore body is known to contain naturally occurring elements of concern such as arsenic, (As), nickel (Ni), molybdenum (Mo), and selenium (Se) which end up concentrated in the tailings after the milling process. The leaching process in the milling operation is done with sulphuric acid and sodium chlorate, at ~pH 1 and prior to the deposition into the tailings facility the pH is increased to ~10 using calcium hydroxide.[9-11] The increased pH prior to deposition in the TMF allows for the precipitation of many of the iron(III) (oxy)hydroxides, and thus containment in the TMF. It is of the utmost importance that the sequestration of EOCs is maintained in the TMFs. The adsorption of EOCs to ferrihydrite is known to sequester these species. The mechanism of this process is important in ensuring the containment of these toxic species to the TMF.

1.3. Ferrihydrite

Ferrihydrite is a highly amorphous unstable iron(III) (oxy)hydroxide, $5Fe_2O_3 \bullet 9H_2O$, which is naturally abundant and was first synthesized by Towe and Bradley.[12] The characterization of this material is known to be difficult due to its disordered state. In general two types of Fh are commonly known and described by the respective X-ray diffraction peaks as 2-line and 6-line ferrihydrite, the latter having a higher degree of crystallinity giving rise to additional diffraction peaks.[3] The formation of Fh is known to occur during the oxidation of aqueous Fe(II) species. Formation occurs in TMFs as the pH of the milling effluent is increased prior to deposition in the TMF. Fh is normally identified as an intermediate state to more stable iron(III) (oxy) hydroxides such as goethite (α-FeOOH) and hematite (α-Fe_2O_3).[3] Fh stability is known to increase upon adsorption of ions and at decreased temperatures in aqueous conditions, leaving Fh relatively stable in TMFs which maintain low temperature ~0°C.[8] The adsorption ability of Fh leads to its importance in the TMFs with the ability to prevent toxic species from entering ground waters. The high surface area of Fh gives it the capability to adsorb many species. However, phase transformations to more stable forms (such as goethite and hematite), leads to a release of adsorbed species which is related to a decrease in the surface area of these more crystalline phases. Transformation of Fh is known to occur due to aging at elevated temperatures, extreme pHs (either high or low), and anoxic (reductive) conditions. Much investigation of the transformation of Fh has been studied due to its role in sequestration of toxic compounds.[1,4,13-19]

Schwertmann and co-workers have created a vast body of work surrounding synthesis, characterization, and behaviour of many iron (oxy)hydroxides. Thermodynamic data was used to relate the stability of ferrihydrite (2-line and 6-line) and schwertmannite (ε-Fe_2O_3) to the degree of crystallinity. This work determined that increased stability comes with an increase in the extent of crystalline phases.[14] Many studies have been performed to relate the transformation of Fh to goethite and hematite as a function of pH. Initial studies determined that the transformation of Fh to hematite occurs at pH between

7 and 8 while goethite was formed at both very high (pH≥12) or very low pH (pH≤4).[4] In addition to the pH dependence of phase transformations, Schwertmann and co-workers also determined that the rate of transformation decreased with decreasing pH.[4,18] Long term studies revealed the transformation of Fh to goethite or hematite was suppressed by increasing adsorption of silicates.[19] Schwertmann found that at increased temperature the transformation to hematite is preferred over goethite and associates this with dehydration, which is required to form hematite.[17] Adsorption studies showed that the greater affinity As has for ferrihydrite over schwertmannite is associated with the higher surface area of Fh.[20] The ability of Fh to adsorb several types of toxic ions is important in the TMFs, but requires comprehensive understanding of the behaviour of the sorbed species and the requirements for desorption of these species. As discussed above, the redox conditions in TMFs could play a critical role in preventing the release of EOCs.

1.4. Elements of Concern – The Importance of Arsenic

Several EOCs are naturally occurring in uranium mine tailings such as Se, Mo, Ni, and As. Arsenic is the center of many investigations due to its toxicity to human and marine life. Arsenic has four stable oxidation states -3, 0, +3, and +5; with limited occurrence of metallic arsenic and -3 only stable at drastically low solution potentials (Eh).[21] As(III) is significantly more toxic than As(V).[21] Most commonly, arsenic is found as oxides, sulfides, and complexes with copper, nickel, iron, and cobalt.[22] Human and animal exposure to arsenic has long been linked to the development of several types of cancer. The importance of understanding the conditions which allow for the sequestration of arsenic on iron (oxy)hydroxides is vital to ensure the protection of ground water. For example, under anoxic (reductive) conditions it is possible that adsorbed As(V) species will be reduced to more labile As(III) with or without the concurrent reductive dissolution of Fh.

To emphasize the pyramidal geometry of arsenate and arsenite, formulas will be displayed in general terms $As(OH)_xO_y$ for the remainder of this thesis. Arsenite (As(III)) is predominately present at low and

slightly basic pH as $As(OH)_3$ (pK_a = 9.2). $As(OH)_2O^-$ (pK_a = 12.7), $As(OH)O_2^{2-}$ and AsO_3^{3-} occur only at very high pHs and low solution potentials ie. reducing conditions, these species have been investigated by Müller *et al*.[23] Arsenite has the highest symmetry (C_{3v}) while in a totally deprotonated or protonated species (refer to Figure 1-1). These species, with C_{3v} symmetry, have two IR active and two Raman active modes, a non-degenerate A_1 mode and a doubly degenerate E mode corresponding to the stretching and deformation vibrations. A reduction in symmetry occurs with deprotonation of this molecule, to C_s which splits the doubly degenerate E mode into the symmetric A' and asymmetric A" modes.[24] The bond length of a protonated As-O bond, As-OH, is slightly longer compared to a deprotonated bond; As-O is a shorter and consequently stronger bond. The As-O vibration is observed at higher frequencies compared to As-OH vibrations.

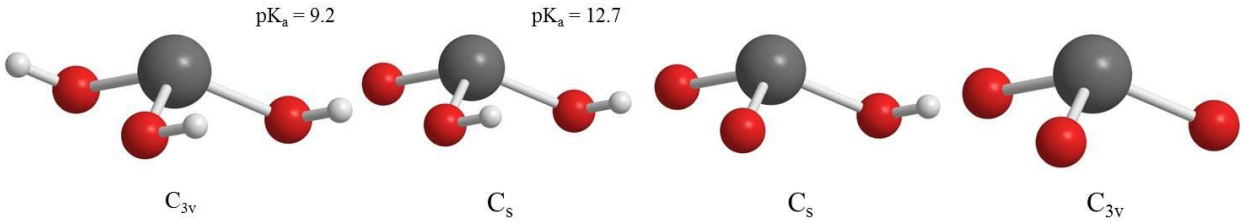

Vibrational Modes				
IR active:	A_1, E	2A', A"	2A', A"	A_1, E
Raman:	$2A_1$, 2E	4A', 2A"	4A', 2A"	$2A_1$, 2E

Figure 1- 1: Arsenite point group symmetry, pK_a, and normal modes of vibration.[25]

Arsenate (As(V)) has several stable species at a range of pHs, AsO_4^{3-}, $As(OH)O_3^{2-}$, $As(OH)_2O_2^-$, and $As(OH)_3O$ with pK_a values at 11.6, 6.8, and 2.3 (refer to Figure 1-2). The totally deprotonated species has the highest symmetry, T_d, which has a triply degenerate, T_2, IR active and Raman active mode along with two additional Raman active modes, non-degenerate A_1 and doubly degenerate E. When this species is protonated there is a reduction of symmetry to C_{3v}, which occurs for two species, $As(OH)O_3^{2-}$ and $As(OH)_3O$. The IR and Raman active T_2 modes are split into non-degenerate A_1 modes and double degenerate E modes. The final species, $As(OH)_2O_2^-$, undergoes an additional loss of symmetry to C_{2v},

which splits the degeneracy of all modes to A_1 and A_2 symmetric, and B_1 and B_2 asymmetric modes. Similar to As(III) species, a deprotonated As-O bond is shorter and stronger in comparison to As-OH which shifts the observed absorption to higher frequencies.

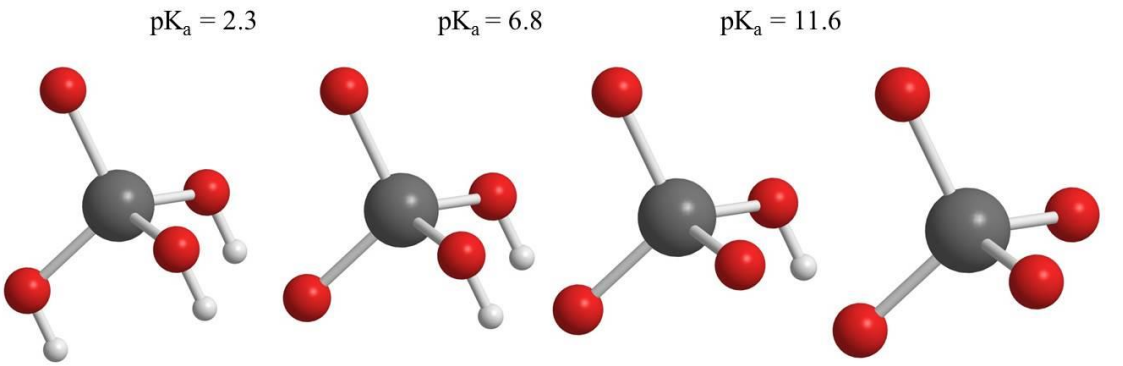

Vibrational Modes

IR active:	A_1, 2E	A_1, B_1, B_2	A_1, 2E	T_2
Raman:	$2A_1$, 2E	$3A_1$, A_2, B_1, B_2	$2A_1$, 2E	A_1, E, T_2

Figure 1- 2: Arsenate point group symmetries, pK$_a$ values, and normal modes of vibration.[25,26]

Mok and Wai investigated the mobility of As(V) and As(III) in the environment and how pH and solubility effect the mobility in areas contaminated by mine wastes.[27] They performed experiments in the absence of oxygen, finding that anaerobic conditions increased the amount of soluble As(V). They attributed this to simultaneous dissolution of iron at these conditions, ultimately the reduction of Fe(III) to Fe(II) which is a more soluble form of iron. This leads to the release of the adsorbed As(V) species.[27,28] They were able to determine that arsenic adsorbed to the surface of iron oxides and could also incorporate into the structure, to form minerals such as scorodite ($FeAsO_4 \bullet 2H_2O$).

Investigation of the structure of adsorbed arsenic species on iron (III) (oxy)hydroxides using extended X-ray absorption fine structure (EXAFS) has been investigated by several researchers. Waychunas *et al*. determined that arsenate forms inner-sphere complexes with several iron(III) (oxy)hydroxides including

ferrihydrite.[29] This bidentate complex was determined to form between two Fe (oxy)hydroxyl octahedra (refer to Figure 1-3). They also found that although mono-dentate complexes did form on Fh they were more common on the more crystalline Fe-(oxy)hydroxides, and most common at low concentrations of arsenic. Fendorf *et al*. determined that surface coverage contributed to the type of complex As formed with goethite.[30] They determined that at low surface coverage arsenate formed primarily mono-dentate complexes while at higher surface coverage both bidentate-mononuclear and bidentate-binuclear complexes were formed. Although they indicated the influence of pH on the system, these authors changed the surface coverage by changing the pH while acknowledging that arsenate protonation will also influence which complex was formed.

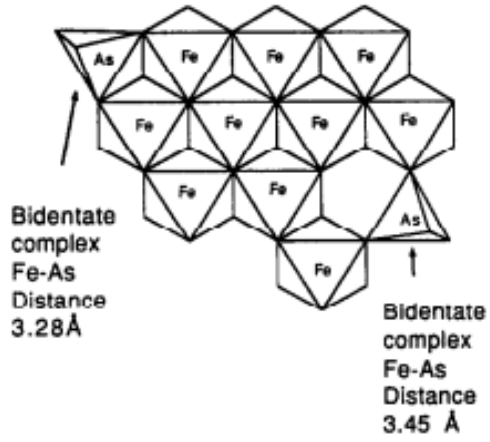

Figure 1- 3: Geometry of As(V) bidentate complex formation on Fh. Adapted from Waychunas *et al*.[29]

Competitive adsorption studies have been used to determine the effect that competing anions have on adsorbed arsenic species. Several studies have investigated the influence of phosphate on iron (oxy)hydroxide adsorbed arsenic species. Carabante *et al.* used competitive adsorption studies to determine that arsenate adsorbed more strongly to ferrihydrite then phosphate.[31] These studies were completed by pre-adsorbing one species and measuring its desorption due to the introduction of an additional species. During this process substantially higher concentrations of phosphate were required to

desorb arsenate, while equal molar concentration of arsenate was sufficient to desorb pre-adsorbed phosphate. Jackson and Miller compared the ability of phosphate and hydroxide to desorb arsenic from goethite and amorphous iron (III) oxides.[32] In general hydroxide was determined to better desorb As species, except in the case of As(V) on goethite and As(III) on amorphous iron oxides where oxidation to As(V) occurred. They determined that phosphate was most prone to competitive desorption at low pHs, around 3. In general these studies have determined that desorption of arsenate is achievable with competing anions. The contribution of anoxic (reductive) conditions is also known to influence the ability of arsenic adsorption.

1.5. Effect of Reductive Conditions

Reductive conditions are known to allow for the release of adsorbed arsenic on iron(III) (oxy)hydroxides.[2,33] In most cases the achievement of reductive conditions is done through potential determining ions or the use of reducing bacteria.[5-7,34-36]

Bacteria have been used in the reduction of several different mineral phases and also in the reduction of arsenic. Smeaton *et al.* used *Shewanella putrefaciens* to measure the release of As and Fe from Pb-As jarosite, an As incorporated mineral phase, $PbFe_3(SO_4,AsO_4)_2(OH)_6$).[5] The use of *Shewanella putrefaciens* in this study arose from its known ability to reduce both As(V) and Fe(III). Smeaton *et al.* determined that Fe(III) reduction to more soluble Fe(II) occurred relatively fast, while the reduction of As(V) was slower and was associated with the release of arsenic during Fe dissolution.[5] Tufano *et al.* used a combination of bacteria in order to differentiate As(V) and Fe(III) reduction.[7] This was done with several strains of *Shewanella sp.*, the ARM1 stain capable of arsenate reduction, and FERM strain capable of iron reduction.[7] In the use of these two *Shewanella sp.* strains they attributed the mobility of As to be more influenced by As reduction than Fe reduction. When comparing As(V) and As(III) release from iron(III) (oxy)hydroxides they determined that the release of As(III) was more prompt. In an additional study by Tufano and Fendorf using an iron reducing bacteria, *Shewanella putrefaciens* for the reduction

of Fh with adsorbed As(III), it was found that after short time periods the Fh initially underwent a phase transformation which actually increased the adsorption of As(III).[6] After increased time, in the presence of bacteria, dissolution of Fe(III) occurred along with concomitant release the As(III). Jones *et al.* investigated the reduction of aqueous and Fe-adsorbed arsenate species using microorganisms also looking at the effects of solution potential.[34] They determined that the reduction of As(V) happened at a rate of 1 mM/d at high concentrations (>600 mM) and at low concentrations of As(V) first-order rates were determined with respect to both concentration and microbial biomass. They performed studies investigating Fe-adsorbed arsenic and monitored the Eh using a Pt electrode. The authors decreased the Eh by purging the oxygen from solution. They determined two behaviours when the Eh decreased from 500 mV to 0 mV on goethite surfaces with respect to surface coverage: At high surface coverage they observed a decrease in aqueous As while at low surface coverage they found an increase in aqueous As. In similar studies on ferrihydrite the aqueous As concentration increased at a faster rate than compared to the presence of goethite.[34] They attribute this to the higher surface area of Fh compared to goethite.[34] Masscheleyn *et al.* studied the redox and pH effects on soluble As in soil.[37] The control of Eh was done using a purge of N_2 or O_2, adapting a procedure previously developed by Patrick *et al.*[37,38] In general they obtained similar findings to other studies. At low pH (<6) and oxidative conditions (>350mV vs NHE), arsenic was predominantly present as As(V) and soluble Mn and Fe were low. Alternatively at higher pH (>6) and reductive conditions between 20 mV and -100 mV, arsenic was reduced to As(III) and the concentration of soluble Mn and Fe increased. They were also able to observe the slow kinetic transformation of As(V)→As(III) by observing soluble As(V) in thermodynamic conditions that favour the presence of As(III).[37]

1.6. Attenuated Total Reflectance –Fourier Transform Infrared

Attenuated total reflection Fourier transform infrared spectrometry (ATR-FTIR) is commonly used for studies investigating interfacial conditions due to its relatively simplistic experimental requirements.

External reflection IR spectroscopy uses a reflective surface, commonly gold in electrochemical experiments. This requires the incident radiation to travel through the electrolyte, reflect and travel back through the electrolyte.[39] Most electrolytes use water a strong absorber of IR radiation as solvent, which requires that the cavity that houses the electrolyte be very thin to allow transmission of the IR radiation. The requirement of the thin cavity introduces a major disadvantage, being mass transport issues in electrochemical experiments. The thin layer is then diffusionally decoupled from the remaining bulk electrolyte.[40] This makes the use of ATR-FTIR beneficial for electrochemical experiments. The sample to be analyzed is placed in direct contact with an internal reflection element (IRE) and does not require the transmission of the incident radiation through the sample; this eliminates the requirement of diluting the sample prior to analysis.[41] Additionally, multi-bounce ATR-FTIR allows for a better signal to noise ratio, an increased signal is observed for each additional bounce within the IRE.

The refraction of radiation when passing between two materials of different refractive indices is described by Snell's law:

$$n_1 sin\theta_1 = n_2 sin\theta_2 \qquad (1\text{-}1)$$

Where n_1 and n_2 are the refractive indices of the two materials and θ_1 and θ_2 are the angle of incidence and refraction. When incident radiation travels from an optically dense material to a material with low refractive index the refracted angle will be greater than the incident angle, $\theta_1<\theta_2$. As the incident angle increases, it approaches an angle where the refraction angle will be 90° with respect to the normal plane , and above this critical angle (θ_c) total internal reflection will occur with the angle of reflection equal to the angle of incidence (refer to Figure 1-4).

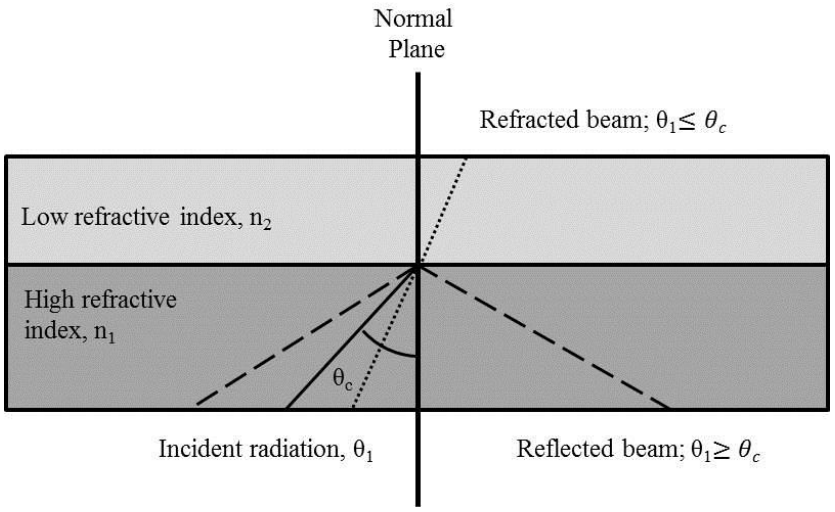

Figure 1- 4: Snell's law, effects of changes in angle of incident radiation.[41]

The use of high refractive index materials is optimal for internal reflection elements (IRE) in ATR experiments. Two common materials used are zinc selenide (ZnSe; n=2.40) and germanium (Ge; n=4.00).

Although the incident radiation is totally internally reflected in the IRE, a photon has an electromagnetic field perpendicular to its momentum vector.[41] The solution of Maxwell's continuity equations at the interface reveals that an evanescent wave must extend beyond the surface of the IRE. The amplitude of the wave decays exponentially from the surface.

$$E(z) = E_0 e^{-\gamma z} \qquad (1\text{-}2)$$

Equation 1-2 relates the strength of the evanescent wave, *E*, with respect to the distance from the surface, *z*, where E_0 is the strength at the surface of the IRE and γ is a constant.[41] The distance in which the evanescent wave can effectively interact with the material at the surface of the IRE is referred to as the depth of penetration, d_p, and is directly influenced by the wavelength of the incident radiation.[41]

$$d_p = \frac{\lambda}{2\pi n_1 \sqrt{sin^2\theta - (n_2/n_1)^2}} \qquad (1\text{-}3)$$

As shown in Equation 1-3, d_p can be quite easily adapted for experimental requirements by changing the angle of incident radiation, θ. For experiments that require larger sensitivity to species in the bulk material a smaller angle of incidence can be used, while if the importance surrounds investigation of the material directly in contact with the IRE a larger angle of incidence should be used. As discussed below, the value of d_p and θ must also be considered when determining the ideal geometry for a particular ATR experiment.

There are many types of IREs with varying geometries which are required depending on experiments to be performed. Single reflection IREs commonly have a hemispherical shape while multi-reflection IREs have a wide variety of shapes and can be single- or double-sided. The absorbance is increased with the increase of each additional reflection which is analogous to creating a longer path length in conventional absorbance spectroscopy. Many optical accessories are available to accommodate different sample types.[41,41,42] Solids normally require a small amount of applied pressure to ensure good contact with the IRE surface and liquids only require some type of containment vessel and possibly a cover depending on the volatility. These varying arrangements allow for vast experimental possibilities for observation with ATR-FTIR.

The use of ATR-FTIR has proved to be popular in interfacial investigations. In many cases the IRE can be coated with a thin film of the material of interest. The thickness of the films needs to be determined based on the requirements of the experiments and is usually based on the d_p. Depending on the experiment, it may be required to investigate the film only or the interaction of a specific species with the film. These different requirements will determine if the film needs to be thick or thin. This technique has been used by many researchers.

Müller *et al*. illustrated the changes in spectra due to changes in the layer of material in the IRE, in their studies of quartz and silica.[43] Their studies were probing the changes in spectral features based on the method of applying the material to the IRE. Specifically they were investigating the effect of material

packing on the IR spectra. To do this they needed to make sure that the layer of material was thicker than the d_p, to ensure the evanescent wave only probes the material of interest and not beyond it. In their study the material on the surface of the IRE was ~7 μm. They were able to observe increased quartz absorbance by increasing the amount of sample in contact with the IRE. This was achieved by wetting and then drying the sample which led to a more densely packed sample. This study identified the importance of particle size and the changes in spectra attributed to it. This is an important consideration for the work in this thesis as Fh will be deposited on the surface of the IRE. As discussed above, if the particle size is too large or non-uniform it will affect the IR response.

The investigation of the solid/liquid interface, specifically the nature of adsorbed species, is often performed using ATR-FTIR. McComb *et al.* were able to determine that antimonate (SbO_4^{3-}) adsorbs to iron oxides by OH^- ligand exchange with the iron oxide surface. They also investigated the desorption behaviour upon increased pH. Yang *et al.* explored the adsorption of catechol on goethite surface using ATR-FTIR with a flow cell along with 2D correlation analysis, and quantum mechanical calculations.[44] 2D correlation analysis is a method which shows the relationship between changing spectral features, and in this case it was used to determine the different types of surface complexes, and the corresponding IR vibrations. Yang *et al.* were able to determine that catechol formed an inner-sphere monodentate structure that is converted to binuclear bidentate complexes under basic conditions. Surface coverage and chromate complexes on ferrihydrite surfaces were studied by Johnston and Chrysochoou, determining that both monodentate and bidentate chromate complexes are formed.[45] These are just a very few examples of the vast possibilities for the use of ATR-FTIR studies, in addition to arsenic adsorption on ferrihydrite.

A substantial amount of work using ATR-FTIR to investigate adsorption of arsenic species on iron(III) (oxy)hydroxides has been performed by Al-Abadleh's group. For example, Depalma *et al.* show the shift in spectra associated with degree of protonation with changes in pH. In this study they investigated the adsorption of p-arsanilic acid (p-AsA) on α- and γ-Fe_2O_3 (hematite and magnetite) and α-

FeOOH (goethite).[46] They observed a shift in absorption frequencies due to the degree of protonation (ie: changing As-O bond length). When p-AsA is adsorbed on iron (III) (oxy)hydroxides the As-O absorption was observed at increased wavenumber from the As-OH absorption.[46] Chabot *et al.* used a flow cell and observed that even at small concentrations, phosphate has the capability to desorb the inner-sphere monodentate complexes of p-AsA from the surface of iron(III) (oxy)hydroxides.[47] In addition, the study by Adamescu *et al.* determined that at neutral pHs Cl^- is capable of desorbing outer-sphere dimethylarsinic acid (DMA) complexes while phosphate at much lower concentrations desorbs at a higher rate.[48] They determined that only at higher concentrations was phosphate capable of desorbing more strongly bound DMA complexes. Mitchell *et al.* used triple-layer surface complex modelling for interpretation of ATR-FTIR spectra to determine the surface complexes being formed.[49] From these fitting models they determined that DMA forms outer-sphere complexes while p-AsA forms inner-sphere complexes with α-Fe_2O_3 and α-FeOOH surfaces. Tofan-Lazar and Al-Abadleh used a flow ATR-FTIR cell to study the adsorption and desorption kinetics of DMA on iron(III) (oxy)hydroxides.[50] This study found the adsorption process of DMA has two contributions; a fast and a slow process. They attributed the fast process to mono-dentate inner-sphere complex formation driven by the electrostatic interaction of the negatively charged DMA species ($(CH_3)_2AsO_2^-$) and the positive $FeOH_2^+$ surface sites which are predominant at pH 7. The slower rates were attributed to the transformation of the monodentate to a bidentate complex, which takes longer to form due to a small likelihood that two fast leaving groups on the iron(III) (oxy)hydroxide surface will be positioned next to each other. The body of work provided by Al-Abadleh highlights the benefits of using ATR-FTIR for the investigation of the formation of surface complexes on iron(III) (oxy)hydroxides.

1.7. Palladium Oxide for pH measurement

Palladium/palladium oxide (Pd/PdO) pH sensors have been developed for many reasons. These sensors are easily miniaturized using Pd wire, which is beneficial when space is limited in the

experimental setup. As will be shown later, measuring pH in a confined geometry is important in this thesis work. Most commonly used ion exchange pH electrodes are sensitive to vibrations and changes in physical orientation, whereas a PdO pH sensor is capable of adaption to harsh conditions.

The Pd-PdO system has been shown to behave according to the following reaction and the pH response is given by the Nernst equation:[51]

$$Pd + H_2O \rightleftharpoons PdO + 2H^+ + 2e^- \qquad (1\text{-}4)$$

$$E = E^o - \frac{RT}{F}[pH] \qquad (1\text{-}5)$$

$$E = E^o - 59mV[pH] at\ RT \qquad (1\text{-}6)$$

It is the sensitivity of the oxide layer to H^+ ions which allows for the pH measurement in this system. The relative ease to make, fast response time, and stability is described by Grubb and King.[52] The ideal potential response according to the Nernst equation gives a slope of -59 mV/pH. Grubb and King were able to prepare many electrodes with close to ideal slopes and a reported standard deviation of ±1.2 mV/pH. They attributed any variation in the slope from the ideal to the possibility of an uneven oxide layer formed on the Pd surface. They determined that these electrodes had 98 % response within the first minute of exposure to electrolyte. The lifetime of these electrodes was determined by long storage times in both dry and neutral pH conditions and it was found that the electrodes maintain ideal pH response up to eight years after preparation. The robustness and lifetime of these electrodes make them particularly appealing for the use in this project for pH measurement during electrochemical experiments.

In practice, good pH response was only attained after particular care and attention to the preparation of the oxidized wire. In particular, the method used to insulate the wire was found to be very important. Specifically, Grubb and King determined the optimal temperature was 800°C in an oxygen swept furnace.[52] Great attention was taken when insulating the wire after the oxidation by removing any oxide from the entire wire except a small amount on the active end. The bare wire then needed to be insulated

in order to ensure only the oxide was exposed to the solution. The importance of this issue will be discussed in Chapters 2 and 3 of this thesis.

1.8. Thesis Objective

The objective of this work was to develop an electrochemical ATR methodology that can relate changes in solution potential to the behaviour of adsorbed arsenic species on the surface of ferrihydrite. This required the development of a spectroelectrochemical cell which was suitable for the necessary experiments. This was previously accomplished in the Burgess group for use with ATR-FTIR on metal films although a completely new cell arrangement and experimental strategy was required for the multi-bounce optics used in this work. This required designing both the spectroelectrochemical cell and the electrodes required for the experiments. The design of a working spectroelectrochemical cell allows for the completion of *in-situ* experiments to observe changes in adsorbed As species with the application of reductive potentials. An additional objective was to successfully develop a method to monitor both the pH and Eh during the experiments to achieve a greater understanding of the exact conditions which alter the adsorption properties of arsenic on ferrihydrite while simultaneously monitoring transformation of ferrihydrite.

Chapter 2 of this thesis describes the experimental procedures used in this work. This includes the synthesis and characterization of Fh, successful design and implementation of the *in-situ* spectroelectrochemical cell, WE configuration, and fabrication of a pH sensitive PdO sensor. Chapter 3 is a discussion of the results from this work. Conclusions and future work will be discussed in Chapter 4.

1.9. Reference List

1. Das, S.; Hendry, M. J.; Essilfie-Dughan, J. *Environ. Sci. Technol.* **2011,** *45*, 268-275.
2. Erbs, J. J.; Berquó, T. S.; Reinsch, B. C.; Lowry, G. V.; Banerjee, S. K.; Penn, R. L. *Geochim. Cosmochim. Acta* **2010,** *74*, 3382-3395.
3. Jambor, J. L.; Dutrizac, J. E. *Chem. Rev.* **1998,** *98*, 2549-2585.
4. Schwertmann, U.; Murad, E. *Clays Clay Miner.* **1983,** *31*, 277-284.
5. Smeaton, C. M.; Walshe, G. E.; Smith, A. M. L.; Hudson-Edwards, K. A.; Dubbin, W. E.; Wright, K.; Beale, A. M.; Fryer, B. J.; Weisener, C. G. *Environ. Sci. Technol.* **2012,** *46*, 12823-12831.
6. Tufano, K. J.; Fendorf, S. *Environ. Sci. Technol.* **2008,** *42*, 4777-4783.
7. Tufano, K. J.; Reyes, C.; Saltikov, C. W.; Fendorf, S. *Environ. Sci. Technol.* **2008,** *42*, 8283-8289.
8. Donahue, R.; Hendry, M. J.; Landine, P. *Appl. Geochem.* **2000,** *15*, 1097-1119.
9. Donahue, R.; Hendry, M. J. *Appl. Geochem.* **2003,** *18*, 1733-1750.
10. Shaw, S. A.; Hendry, M. J.; Essilfie-Dughan, J.; Kotzer, T.; Wallschläger, D. *Appl. Geochem.* **2011,** *26*, 2044-2056.
11. Moldovan, B. J.; Hendry, M. J.; Harrington, G. A. *Appl. Geochem.* **2008,** *23*, 1437-1450.
12. Towe, K. M.; Bradley, W. F. *J. Colloid Interface Sci.* **1967,** *24*, 384-392.
13. Das, S.; Hendry, M. J. *Chem. Geol.* **2011,** *290*, 101-108.
14. Majzlan, J.; Navrotsky, A.; Schwertmann, U. *Geochim. Cosmochim. Acta* **2004,** *68*, 1049-1059.
15. Schwertmann, U.; Friedl, J.; Kyek, A. *Clays Clay Miner.* **2004,** *52*, 221-226.
16. Schwertmann, U. *Plant and Soil* **1991,** *130*, 1-25.
17. Schwertmann, U.; Friedl, J.; Stanjek, H. *J. Colloid Interface Sci.* **1999,** *209*, 215-223.
18. Schwertmann, U.; Stanjek, H.; Becher, H.-H. *Clay Miner.* **2004,** *39*, 433-438.
19. Schwertmann, U.; Friedl, J.; Stanjek, H.; Schulze, D. G. *Clay Miner.* **2000,** *35*, 613-623.

20. Carlson, L.; Bigham, J. M.; Schwertmann, U.; Kyek, A.; Wagner, F. *Environ. Sci. Technol.* **2002,** *36*, 1712-1719.

21. Ferguson, J. F.; Gavis, J. *Water Res.* **1972,** *6*, 1259.

22. Canadian Soil Quality Guidlines for the Protection of Environmental and Human Health: Arsenic (inorganic). *Canadian Council of Minister of the Environment* **2001**.

23. Müller, K.; Ciminelli, V. S. T.; Dantas, M. S. S.; Willscher, S. *Water Res.* **2010,** *44*, 5660-5672.

24. Loehr, T. M.; Plane, R. A. *Inorg. Chem.* **1968,** *7*, 1708-1714.

25. Carter, R. L. *Molecular Symmetry and Group Theory;* John Wiley and Sons, Inc.: 1998.

26. Goldberg, S.; Johnston, C. T. *J. Colloid Interface Sci.* **2001,** *234*, 204-216.

27. Mok, W. M.; Wai, C. M. *Wat. Res.* **1989,** *23*, 7-13.

28. Deuel, L. E.; Swoboda, A. R. *Soil Sci. Soc. Proc.* **1972,** *36*, 276-278.

29. Waychunas, G. A.; Rea, B. A.; Fuller, C. C.; Davis, J. A. *Geochim. Cosmochim. Acta* **1993,** *57*, 2251-2269.

30. Fendorf, S.; Eick, M. J.; Grossl, P.; Sparks, D. L. *Environ. Sci. Technol.* **1997,** *31*, 315-319.

31. Carabante, I.; Grahn, M.; Holmgren, A.; Hedlund, J. *J. Colloid Interface Sci.* **2010,** *351*, 523-531.

32. Jackson, B. P.; Miller, W. P. *Soil Sci. Soc. Am. J.* **2000,** *64*, 1616-1622.

33. Smith, E.; Naidu, R.; Alston, A. M. *Adv Agron* **1998,** *64*, 149-195.

34. Jones, C. A.; Langner, H. W.; Anderson, K.; McDermott, T. R.; Inskeep, W. P. *Soil Sci. Soc. Am. J.* **2000,** *64*, 600-608.

35. LaKind, J. S.; Stone, A. T. *Geochim. Cosmochim. Acta* **1989,** *53*, 961-971.

36. Langner, H. W.; Inskeep, W. P. *Environ. Sci. Technol.* **2000,** *34*, 3131-3136.

37. Masscheleyn, P. H.; Delaune, R. D.; Patrick, W. H. *Environ. Sci. Technol.* **1991,** *25*, 1414-1419.

38. Patrick, W. H.; Williams, B. G.; Moraghan, J. T. *Soil Sci. Soc. Am. J.* **1973,** *37*, 331-332.

39. Griffiths, P. R.; de Haseth, J. A. Specular Reflection. In *Fourier Tansform Infrared Spectrometry*, John Wiley & Sons, Inc.: Hoboken, NJ, 2007; pp 277-301.

40. Bae, I. T.; Sandifer, M.; Lee, Y. W.; Tryk, D. A.; Sukenik, C. N.; Scherson, D. A. *Anal. Chem.* **1995,** *67*, 4508-4513.

41. Griffiths, P. R.; de Haseth, J. A. Attenuated Total Reflection. In *Fourier Transform Infrared Spectrometry*, 2nd ed.; John Wiley & Sons, Inc.: Hoboken, NJ, 2007; pp 321-348.

42. Harrick, N. J. *Appl. Opt.* **1966,** *5*, 1-2.

43. Müller, C. M.; Molinelli, A.; Karlowatz, M.; Aleksandrov, A.; Orlando, T.; Mizaikoff, B. *J. Phys. Chem. C* **2012,** *116*, 37-43.

44. Yang, Y.; Yan, W.; Jing, C. *Langmuir* **2012,** *28*, 14588-14597.

45. Johnston, C. P.; Chrysochoou, M. *Environ. Sci. Technol.* **2012,** *46*, 5851-5858.

46. Depalma, S.; Cowen, S.; Hoang, T.; Al-Abadleh, H. A. *Environ. Sci. Technol.* **2008,** *42*, 1922-1927.

47. Chabot, M.; Hoang, T.; Al-Abadleh, H. A. *Environ. Sci. Technol.* **2009,** *43*, 3142-3147.

48. Adamescu, A.; Mitchell, W.; Hamilton, I. P.; Al-Abadleh, H. A. *Environ. Sci. Technol.* **2010,** *44*, 7802-7807.

49. Mitchell, W.; Goldberg, S.; Al-Abadleh, H. A. *J. Colloid Interface Sci.* **2011,** *358*, 534-540.

50. Tofan-Lazar, J.; Al-Abadleh, H. A. *J. Phys. Chem. A* **2012,** *116*, 1596-1604.

51. Karagounis, V. A.; Liu, C. C.; Neuman, M. R.; Romankiw, L. T.; Leary, P. A.; Cuomo, J. J. *IEEE Trans. Biomed. Eng.* **1986,** *BME-33*, 113-116.

52. Grubb, W. T.; King, L. H. *Anal. Chem.* **1980,** *52*, 270-273.

2. Experimental

2.1. Reagents

Potassium chloride (KCl, >99%), sodium arsenate dibasic heptahydrate ($NaHAsO_4$, >98%), iron sulfate hydrate ($Fe_2(SO_4)_3xH_2O$, 21-23% Fe), sodium (meta) arsenite, ($NaAsO_2$, JT Baker), and potassium sulfate (K_2SO_4, 99.0%) were all used as received. Solutions were made from MilliQ water (>18.2 MΩ cm^{-1}) or deuterium oxide (99.9 atom % D).

2.2. Ferrihydrite

2.2.1. Synthesis

A modified version from Schwertmann and Cornell was used for the synthesis of ferrihydrite.[1] A 0.2 M solution of iron(III) sulfate ($Fe_2(SO_4)_3$) was adjusted to pH 7 using a 1 M NaOH solution and stirred for an hour. This solution was washed several times with MilliQ water before pressure filtering with a 0.22 μm filter. After filtering, the precipitate was dried in air for several days before pulverizing with a mortar and pestle. The chemical formula for Fh is reported as $5Fe_2O_3 \cdot 9H_2O$, where the adsorption of several types of species is common by the replacement of water and the FeOH and $FeOH_2^+$ surface sites.[2-4] Due to the ability of Fh to easily adsorb species a portion of SO_4^{2-} remains adsorbed to the Fh surface after synthesis, the sulfate source being the $Fe_2(SO_4)_3$ starting material. Carbonate (CO_3^{2-}) was also found to be adsorbed to the Fh surface, which is commonly found when synthesis is performed under atmospheric conditions.[5] This occurs by the conversion of dissolved CO_2 to CO_3^{2-} as the pH is increased during the precipitation of Fh.

2.2.2. Characterization

Several methods to identify the synthesis of ferrihydrite were used, including powder X-ray diffraction (pXRD), ATR-FTIR, and Raman spectroscopy. Characterization using only XRD is difficult due to the limited number of identifiable peaks with broad low intensity features, which is due to the short range order of Fh. For this reason additional methods, such as ATR-FTIR and Raman spectroscopy, are used in the identification process of Fh.

2.2.2.1. Ferrihydrite Deposition

Ferrihydrite was deposited on the IRE surface using the following procedure. A colloidal mixture of Fh and D_2O was made, with ~17.5 mg of Fh in 5 mL of D_2O. This mixture was sonicated to suspend the Fh particles in solution and 0.6 mL of this solution was deposited on the surface of the IRE and allowed to air dry. The Fh deposited on the ZnSe IRE is shown in more detail with an optical image in Figure 2-1. As discussed in the Introduction, when using ATR-FTIR to study a material deposited on the surface on the IRE it is important to understand the Fh thickness and the d_p. The majority of experiments performed in this work are investigating the adsorption of arsenic species on the surface of Fh. For this reason if the Fh layer was substantially thicker than the d_p the evanescent wave would not be able to investigate the adsorption processes at the surface of the Fh. An approximate Fh thickness was found to be 1.4 μm, using the following information: Fh density of 3.5 g/cm^3 and an exposed surface of the IRE of 5.4 cm x 0.8 cm along with the colloidal solution information given above.[10] Confirmation of the Fh layer thickness was done using profilometery and found to be between 1.0 and 1.6 μm. This Fh thickness ensures that the entire Fh surface is being probed by the evanescent wave and there is minimal penetration beyond the Fh surface, based on the 1.6 μm d_p calculated using Equation 1-3 with an angle of incidence of 40°.

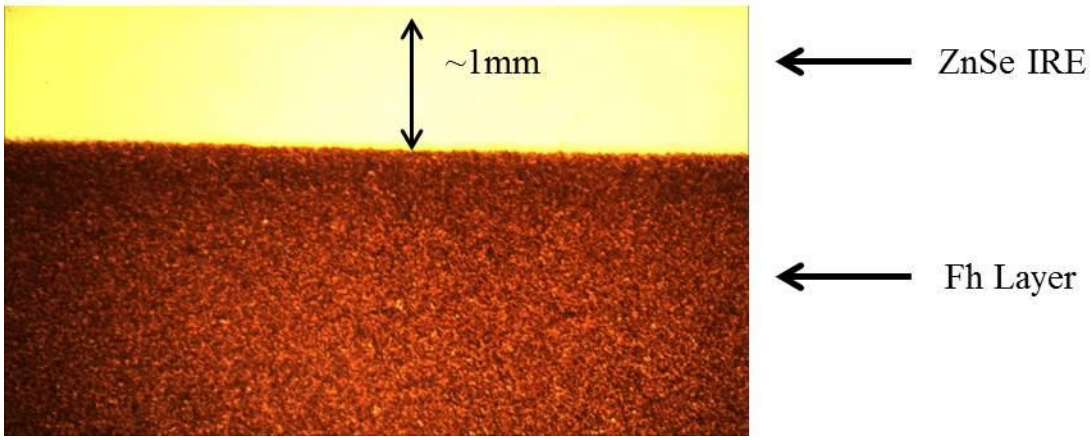

Figure 2- 1: Optical image at 10x zoom of Fh deposited on ZnSe IRE.

2.2.2.2. XRD

XRD analysis was performed at the Cameco research facility in Port Hope, Ontario. XRD was performed using a Rigaku Ultima IV with a Cu source scanning from 5 to 80 degrees with a step size of 0.03 degrees and 5 seconds per step. These long scanning times are required for amorphous samples, such as Fh, in order to obtain high enough intensities to observe the weak diffraction peaks. Characterization of 2-line Fh was determined by the two diffraction peaks at 2θ of 34° and 61° (refer to Figure 2-2).[6,7]

2.2.2.3. ATR-FTIR

Thermo Nicolet Nexus 870 FT-IR spectrometer equipped with ATRMaxII multi-bounce optics was used for all IR measurements performed in this thesis. All experiments used either a ZnSe (refractive index 2.4) IRE with dimensions of 56x10x4 mm and a 45° beveled angle or a Ge (refractive index 4.0) IRE with the same dimensions. Measurements were taken with 4 cm^{-1} resolution and 64 co-added scans at a 40° angle of incidence, unless otherwise specified. All ATR-FTIR spectra collected in this thesis are displayed as:

$$\frac{\Delta S}{S} = \frac{S_{sample} - S_{reference}}{S_{reference}} \qquad (2\text{-}1)$$

S represents the single beam measurement. This method of analysis calculates the relative change in the IR signal between a reference and sample spectrum. In this method of analysis a positive absorbance band represents a loss of species from the surface of the IRE, while negative absorbance represents an increase in the species at the surface of the IRE.

The ATR-FTIR spectrum of ferrihydrite is shown in Figure 2-3. The Fh preparation method and deposition on the IRE is described above. The main IR feature is observed at ~700 cm^{-1} and is attributed to the Fe-O vibration, an additional Fe-O IR active feature should be observed at ~500 cm^{-1} although, due

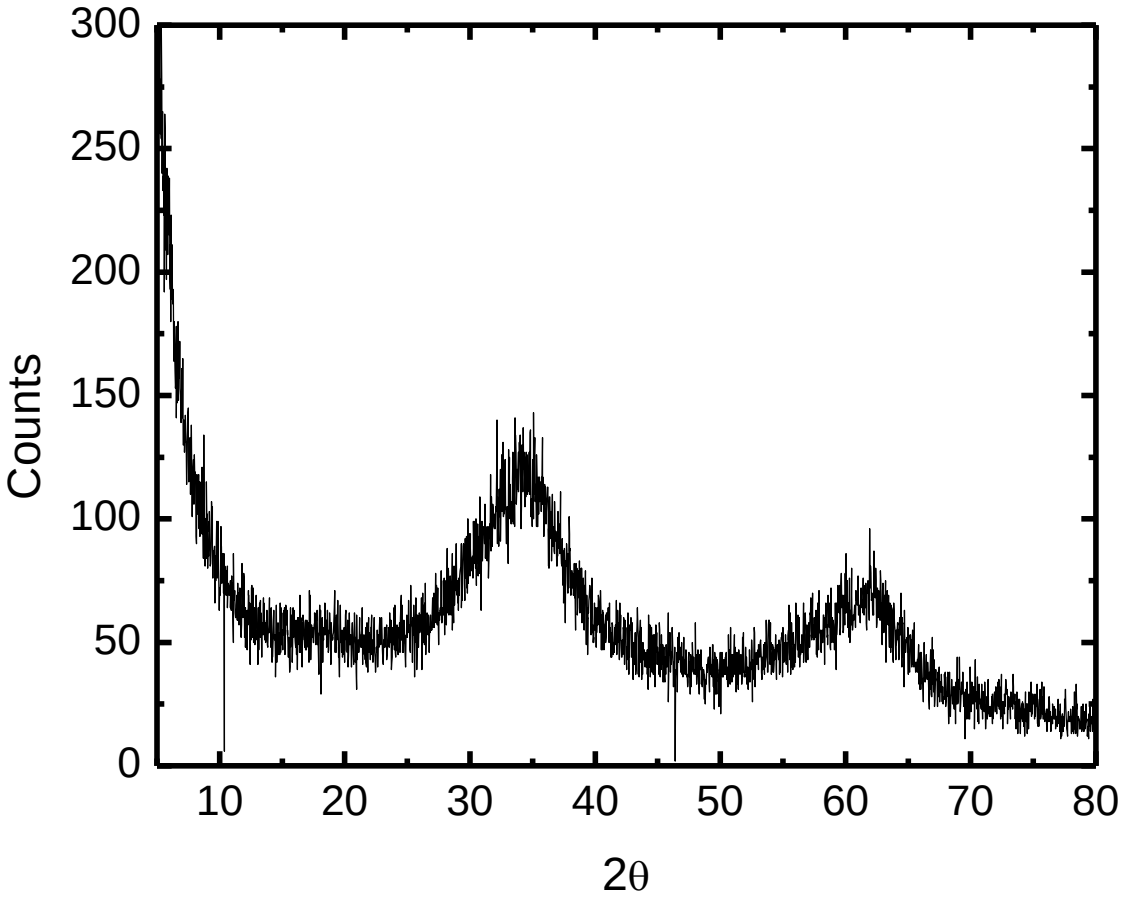

Figure 2- 2: XRD characterization of 2-line Fh. Using Rigaku Ultima IV with a Cu source scanning from 5 to 80 degrees with a step size of 0.03 degrees and 5 seconds per step.

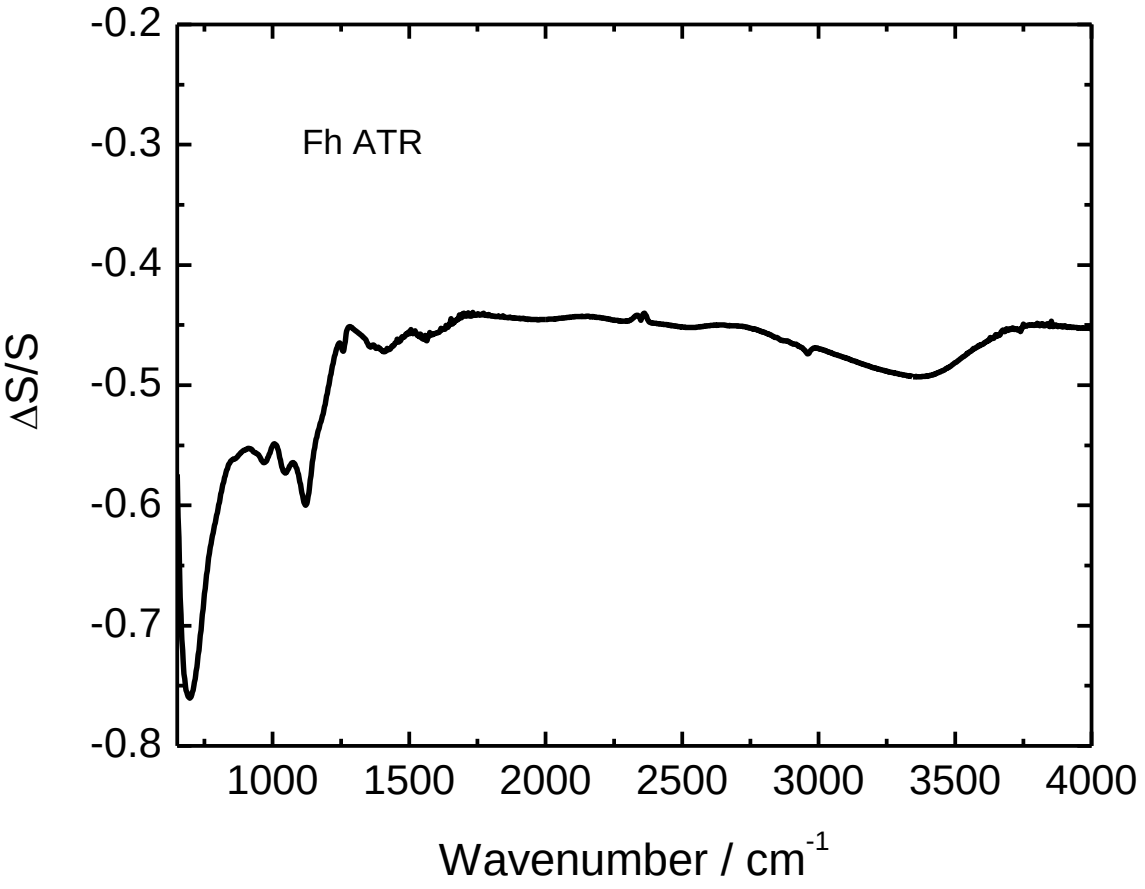

Figure 2- 3: ATR-FTIR spectra of 2-line Fh. Reference spectrum: clean dry ZnSe; Sample spectrum: Fh coated ZnSe.

to the ZnSe cut-off, this band is not observed in this work.[8] Additional bands associated with adsorption of water and surface OH stretching groups are observed at ~1600 cm^{-1} and 3400 cm^{-1}.[8,9] Additional low intensity bands between 850 cm^{-1} and 1500 cm^{-1} are associated with CO_3^{2-} and SO_4^{2-} modes.

2.2.2.4. Raman

Raman spectra were measured using a Renishaw Raman Microscope with a 514 nm laser at 5 % and 10 % power. Prior to analysis the sample was ground with a mortar and pestle. Das *et al.* determined the highest intensity Fh Raman active band at 707 cm^{-1}, along with two additional low intensity bands at 361 cm^{-1} and 508 cm^{-1}.[6] The Raman spectra collected for this work (Figure 2-4, black line) has the highest intensity band at ~709 cm^{-1} with very small contribution at 357 cm^{-1}. At a higher laser power, 10 %, characteristic peaks from hematite were observed (refer to Figure 2-4, grey line). As reported by Das *et al.* the highest intensity Raman active bands for hematite are at 222 cm^{-1} and 290 cm^{-1}, these bands are observed at 216 cm^{-1} and 287 cm^{-1} in this study.[6] This phase transformation is also observed in pictures that were taken before and after the Raman spectra were measured. There is an area in which the sample underwent phase transformation to hematite (based on the Raman spectra) due to the focus of the laser, which can be observed as a darker brown colour in Figure 2-5. This colour change is slightly noticeable at 5 % laser power, and a 10 % laser power the colour change is much more significant.

2.3. ATR-FTIR - Open Circuit Conditions

2.3.1. As(V) in solution

A clean (ie. uncoated) IRE was used for experiments to observe As(V) in solution. At neutral pHs the ZnSe IRE element was used at an angle of incidence (AOI) of 40°. The depth of penetration of the evanescent wave for experiments using the ZnSe IRE is determined to be 1.61μm with a total of 7 bounces at the surface of the IRE, calculated using Equation 1-3. Due to the instability of ZnSe outside

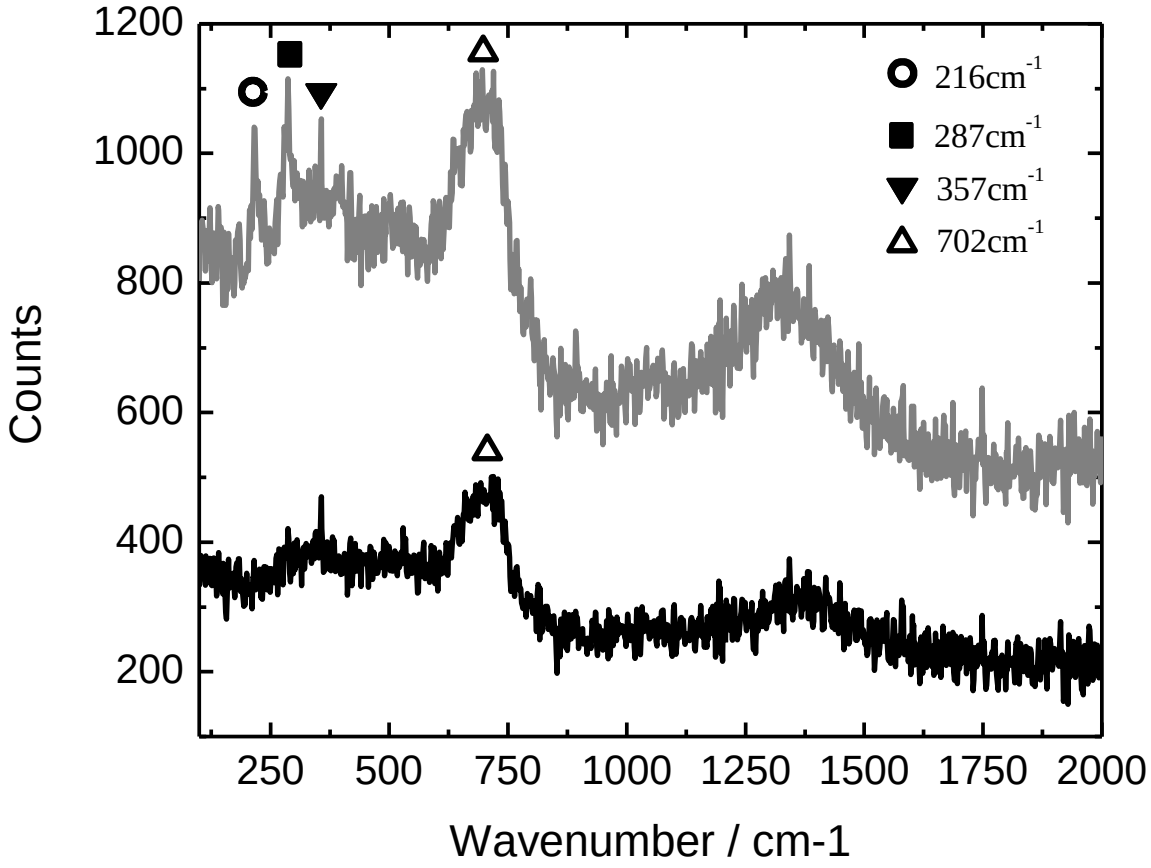

Figure 2- 4: Raman spectra for characterization of 2-line ferrihydrite. Measurements taken with 514 nm laser at 5 % power (black line) and 10 % power (grey line). Higher power scan (grey line) indicates transformation to hematite.

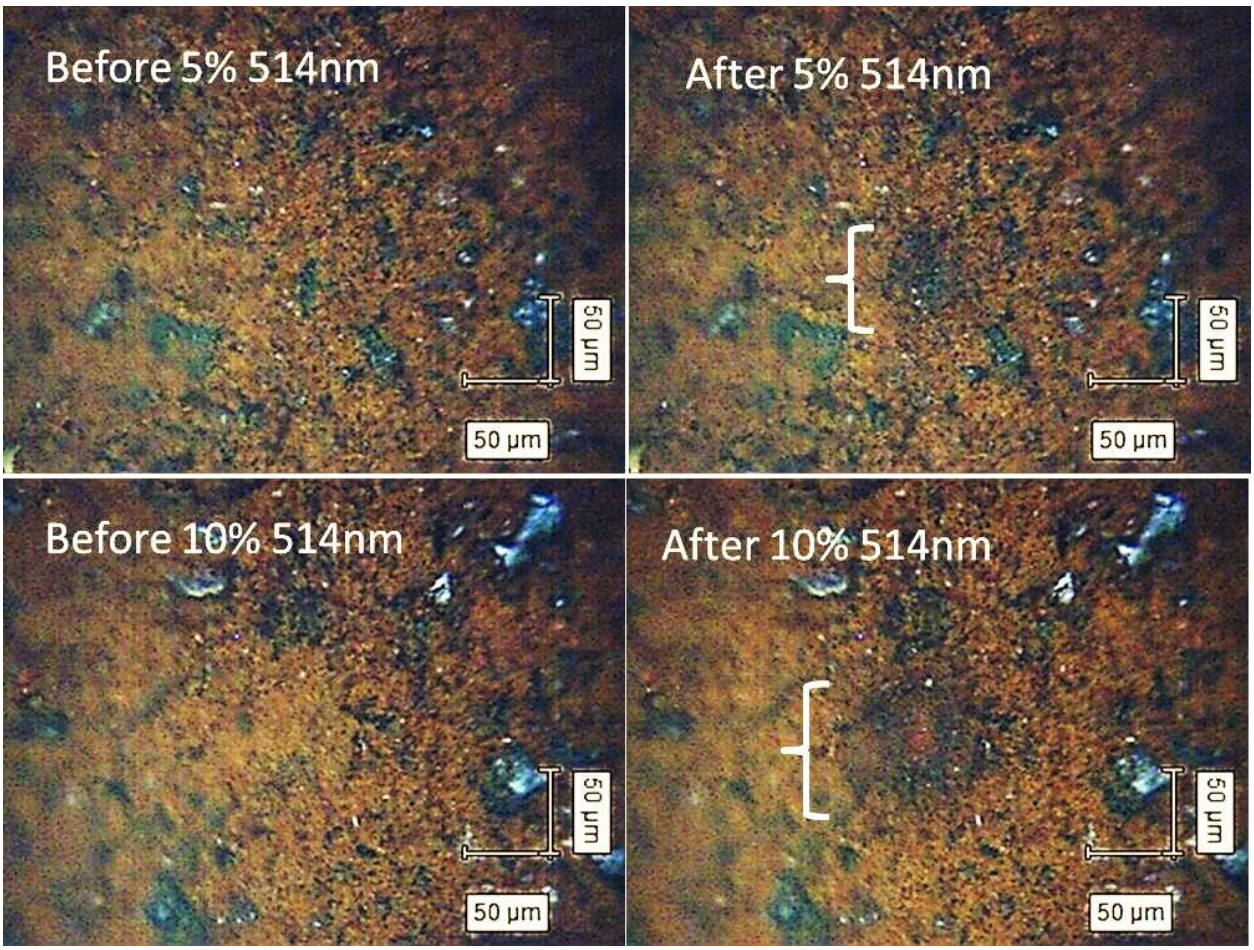

Figure 2- 5: Before and after Raman measurements to visually show the transformation of Fh to hematite. With 514 nm laser at 5 % power there is a very slight dark spot while at 10 % a more significant portion of the sample underwent phase transformation.

the pH range of 5-10 the Ge IRE was used for experiments at high and low pH. For ATR-FTIR experiments using the Ge IRE, a 25° AOI was used, making the d_p for these experiments 0.71 μm with 8 bounces at the surface of the IRE. These calculations are done for 1000 cm^{-1}, and a sample refractive index equal to that of water.

2.4. ATR-FTIR – Spectroelectrochemistry

All spectroelectrochemical experiments were performed using a Brinkmann Wenking LT 73 Potentiostat. The electrodes used in these experiments are described below and the electrolyte consisted of 5 mM K_2SO_4 solution in D_2O.

2.4.1. Method Development

The use of spectroelectrochemistry is extremely suitable for the work in this thesis, in order to observe *in-situ* electrochemical changes to Fh-adsorbed As species. Since there are no commercially made spectroelectrochemical cells for the type of experiments required for this body of work an in-house design was required.

2.4.1.1. Cell Design

When designing this cell many aspects of the experimental requirements had to be considered. The cell had to seal to the IRE and still have a sufficient available exposed IRE surface to allow the appropriate electrochemical experiments to be performed. The cell also needed to have enough space for the required electrodes along with ports for purging the cell with an inert gas (Ar).

Initially, a new trough to house the IRE needed to be made, which required a means to fasten the cell onto the trough (refer to Figure 2-6). The design of the trough was based on the commercial trough

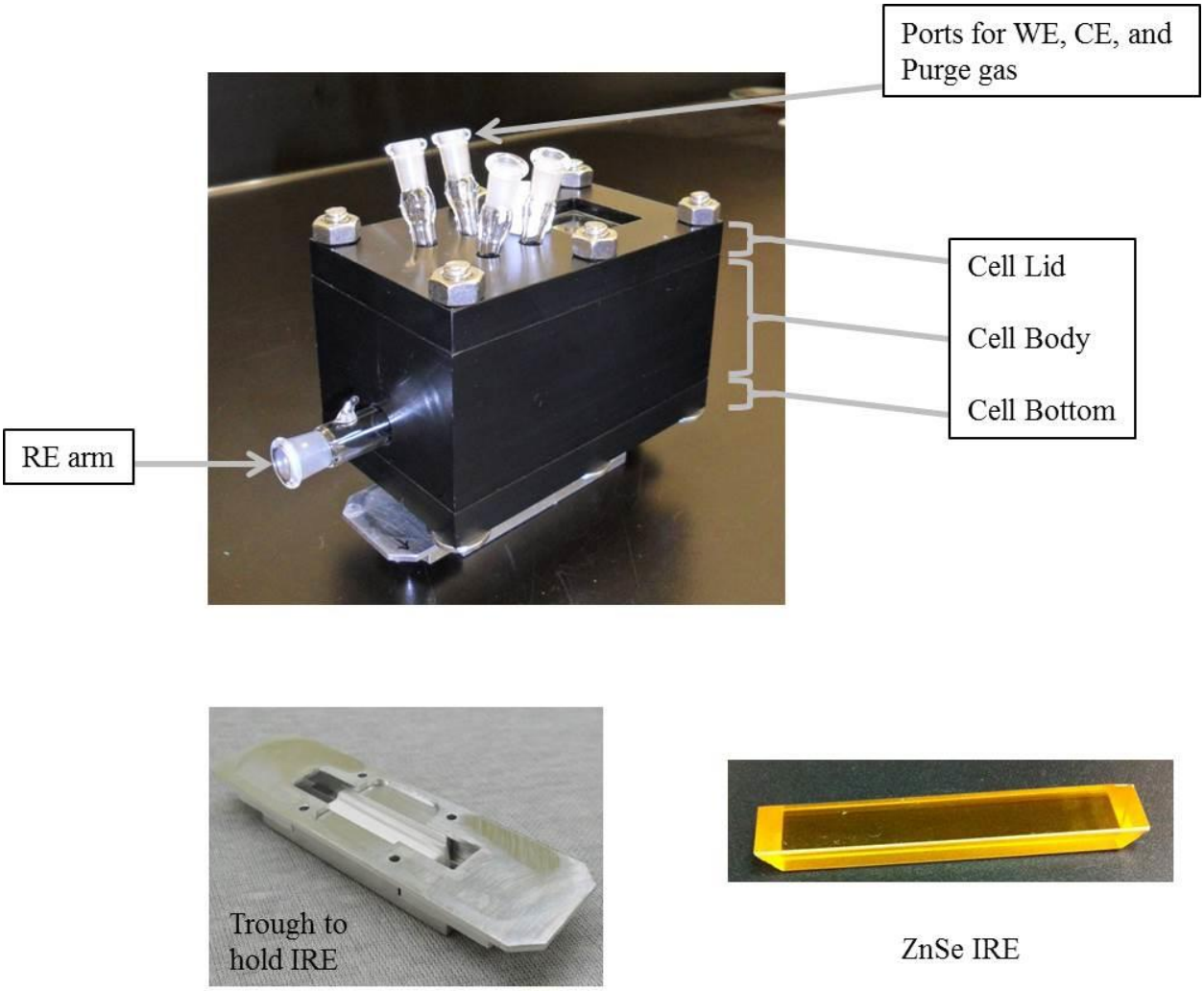

Figure 2- 6: Spectroelectrochemical final cell design along with ZnSe IRE and trough.

which came with the multi-bounce optics.

The spectroelectrochemical cell was fabricated from Delrin and was designed in three portions; the cell bottom which fastened to the surface of the IRE, the cell body, and the cell lid (refer to Figure 2-6 for a picture of the assembled cell). The IRE is sealed to the cell bottom with a 1 mm thick chemical resistance rubber gasket, which overlapped the IRE by 1 mm on all sides. This orientation allowed for 54x8 mm of exposed IRE surface after assembling the cell. The cell body is then fastened to the bottom and sealed with an O-ring, with a port on the side for the reference electrode. These two portions of the cell made it possible for several cell volumes depending on the experiment. Experiments performed at atmospheric conditions could be done with just the cell bottom (~8 mL volume) or the addition of the cell body if larger volumes were required, ~30 mL. The side of the cell body is equipped with an adapted port in order to allow a salt bridge for the reference electrode. For experiments that require oxygen free conditions, the cell lid is fastened to the body and sealed with an additional O-ring. The cell lid is equipped with ports to accommodate the working electrode, counter electrode, and purge gas, in addition to a viewing window.

2.4.1.2. Electrodes

The initial working electrode design was based on previous experiments performed in the Burgess group using attenuated total reflectance surface enhanced infrared absorption spectroscopy (ATR-SEIRAS).[11] These experiments used electroless deposition of a gold working electrode (WE) on the surface of a silicon (Si) hemisphere IRE. This method coats the IRE with a thin conductive layer of Au which is contacted with a gold wire for electrochemical control. The method used for deposition of Au on the Si surface requires the use of a HF solution but; due to the instability of ZnSe in the presence of acid this method was not suitable for work in this thesis. As an alternative, a thin layer of gold was sputtered on the surface of the ZnSe IRE. Although this method provided a conductive layer of gold, it proved to be too reflective which reduced the penetration of the evanescent wave beyond the surface of

the IRE. This result warranted need for a different design for the WE used in the spectroelectrochemical experiments. The new design used a rectangular block of Ni which was slightly smaller than the IRE exposed surface, a contact bar was tapped in the Ni block and used to lower the block onto the surface of the Fh from above (refer to Figure 2-7 for schematic of the cell setup).

The Ni block was gold plated using a modified method from Kohl.[12] The electroplating solution was comprised of 0.15 M $NaAu(CN)_2$, and ~100 g/L citric acid, the pH was adjusted to ~3.5. A current of -95 mA was applied to the Ni block, with a surface area of ~12.9 cm^2, giving a current density of ~7.2 mA/cm^{-2}. The electrochemical treatment continued until the entire surface was covered with a thin layer of Au.

2.4.1.3. Fh stability related to Solution Concentration

The Fh drop casting method (described above) on the ZnSe IRE left the Fh very stable on the surface of the IRE, which could only be removed after abrasion. It was found that during some experiments the Fh would lift off the surface of the IRE during a disturbance, such as the lowering of the WE block. Several beaker experiments were performed to determine if the total concentration had an effect on the stability of the Fh layer. A Fh layer was deposited on a ZnSe window and placed in solutions with different concentrations of sulfate and arsenate. The initial experiment placed the Fh covered ZnSe in a beaker of water and the Fh remained very stable. No Fh was removed from the ZnSe during agitation of the solution. With the gradual increase in ionic strength the Fh stability decreased. The next two experiments exposed the Fh covered ZnSe to 5.9mM SO_4^{2-} and a combination of 4.9mM As(V) and 5.4 SO_4^{2-}. Both of these Fh layers remained on the ZnSe surface during solution agitation. Upon increasing the concentrations to 6.8mM SO_4^{2-} and 20.8 mM As(V) most of the Fh layer lifted off the ZnSe over a period of ~3 hours during solution agitation. Presumably this observed instability is related to surface coverage. When the total surface coverage of adsorbed species increases the Fh is simply lifted off the ZnSe surface.

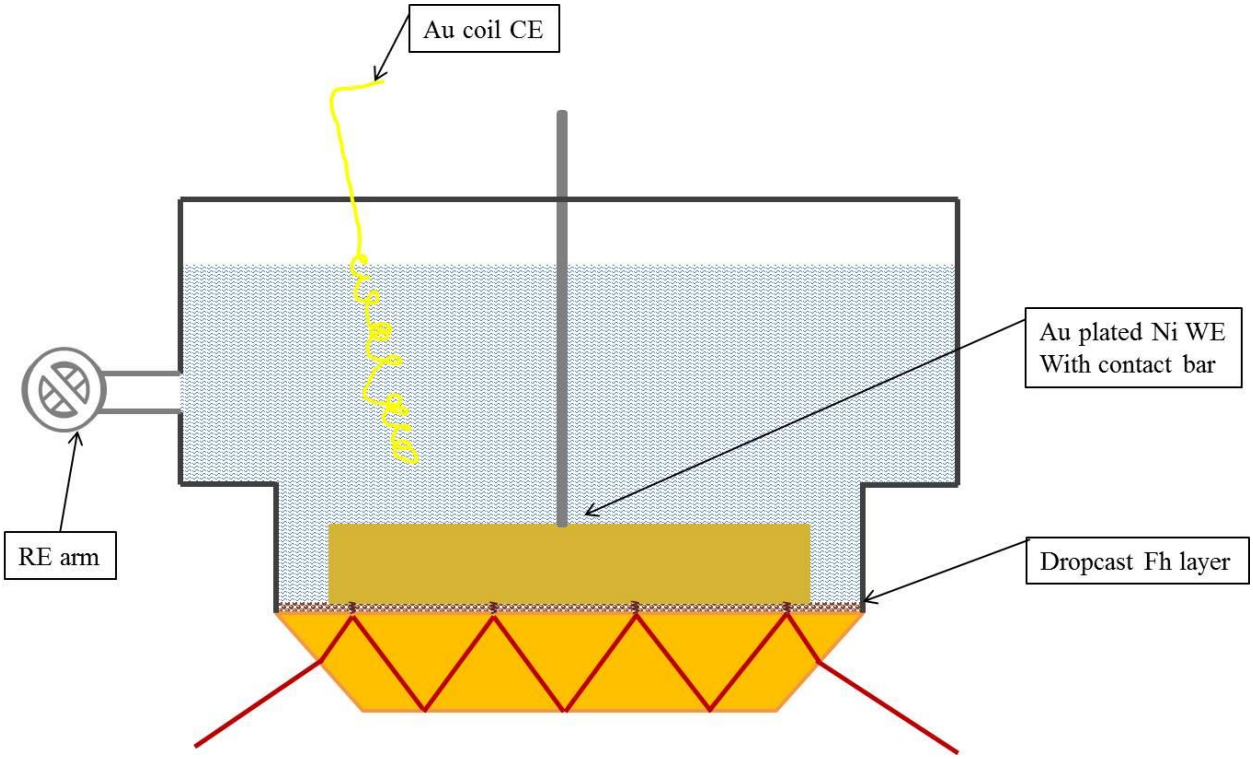

Figure 2- 7: Schematic of final design of spectroelectrochemical cell setup.

2.5. Electrochemistry

Cyclic voltammetry (CV) was used to determine the potential required to reduce Fe(III) in ferrihydrite. These experiments were performed using a Heka potentiostat PG 590. In these experiments the potential was swept between 100 mV and -900 mV at a scan rate of 50 mV/sec. The electrolyte used was a degassed 0.1 M KCl solution. The working electrode was a nickel disk with ~5 mm diameter. A potential cycle with an unmodified WE was used to determine any changes due to Ni redox. To determine the potentials required to reduce Fe(III) a layer of Fh was drop cast on the surface of the WE. Additional electrodes used were a Pt coil counter electrode (CE) and a saturated KCl Ag/AgCl reference electrode (RE).

2.6. pH and Eh Measurements

The potential monitoring required for these experiments was done with an in-house monitor program. The programs were written in the LabVIEW program environment. The potential application was performed using a Heka potentiostat P590.

2.6.1. PdO Preparation for pH sensing

Palladium wire used for the development of the pH sensors was supplied from Sigma-Aldrich (99.9% trace metal basis) with a 0.5 mm diameter. The preparation procedure used was slightly modified from Grubb and King.[13] Prior to the heating process the wires were cut to the desired length, (approximately 3 cm), and the end which was to be oxidised was rounded using a wet stone. The rounded end was then dipped in aqua regia for 20 seconds, rinsed with MilliQ, dipped in 50 % NaOH and dried in a flow of argon gas for approximately 10 minutes.

Three generations of PdO wires were fabricated to determine the feasibility for use in measuring changes in pH. The preparation, prior to heating, given above was used for each generation of wires. The

first generation wire was placed in an oven at 750°C for 20 minutes in air. The second generation consisted of two wires which were heated using the following heating method. The wires were placed in the oven at 600°C and then the oven was purged with O_2, the temperature was increased to 750°C at 2.5 degrees/minute, then held at 750°C for 20 minutes, the wires were then air quenched. The third generation of wires used three different heating procedures to determine if there was an optimal heating method for better pH sensitivity. The heating cycles implemented were 750°C for 20 minutes, 750°C for 40 minutes, and 800°C for 20 minutes. In each of these procedures the oven was heated to the desired temperature before the wires were placed in the oven. The oven was purged with oxygen prior to and during each of the heating cycles and the wires were air quenched after being in the oven for the required time. After removal from the oven the oxidized end of the wire was a dark grey to black colour. The entire wire was scraped with a razor blade in order to remove all the oxide from the surface of the wire except for approximately 3 mm at the prepared end of the wire. The wire was then insulated to ensure the bare wire was isolated; this was done with a heat shrink plastic which was sealed to the wire with a small amount of epoxy. This process was done to ensure that the oxidized portion of the palladium wire was the only portion that was exposed to solution for the pH measurements.

The oxide layers which were formed on the palladium surface were observed using an optical microscope prior to testing each electrode. Based on the visual inspection of the oxide layers it appeared that the wires heated at 800°C for 20 minutes had a consistent oxide layer, which appeared as a black oxide. The wires which were heated at 750°C for 20 minutes appeared to have a less consistent oxide layer, shown with spots that were metallic silver as opposed to a black or charcoal oxide layer (refer to Figure 2-8). The literature indicated that any inconsistency in the oxide layer would affect the pH response of the palladium oxide, but in this case the electrodes have near ideal pH response.[13] The pH response of the individual electrodes will be discussed in greater detail in the Results section of this thesis.

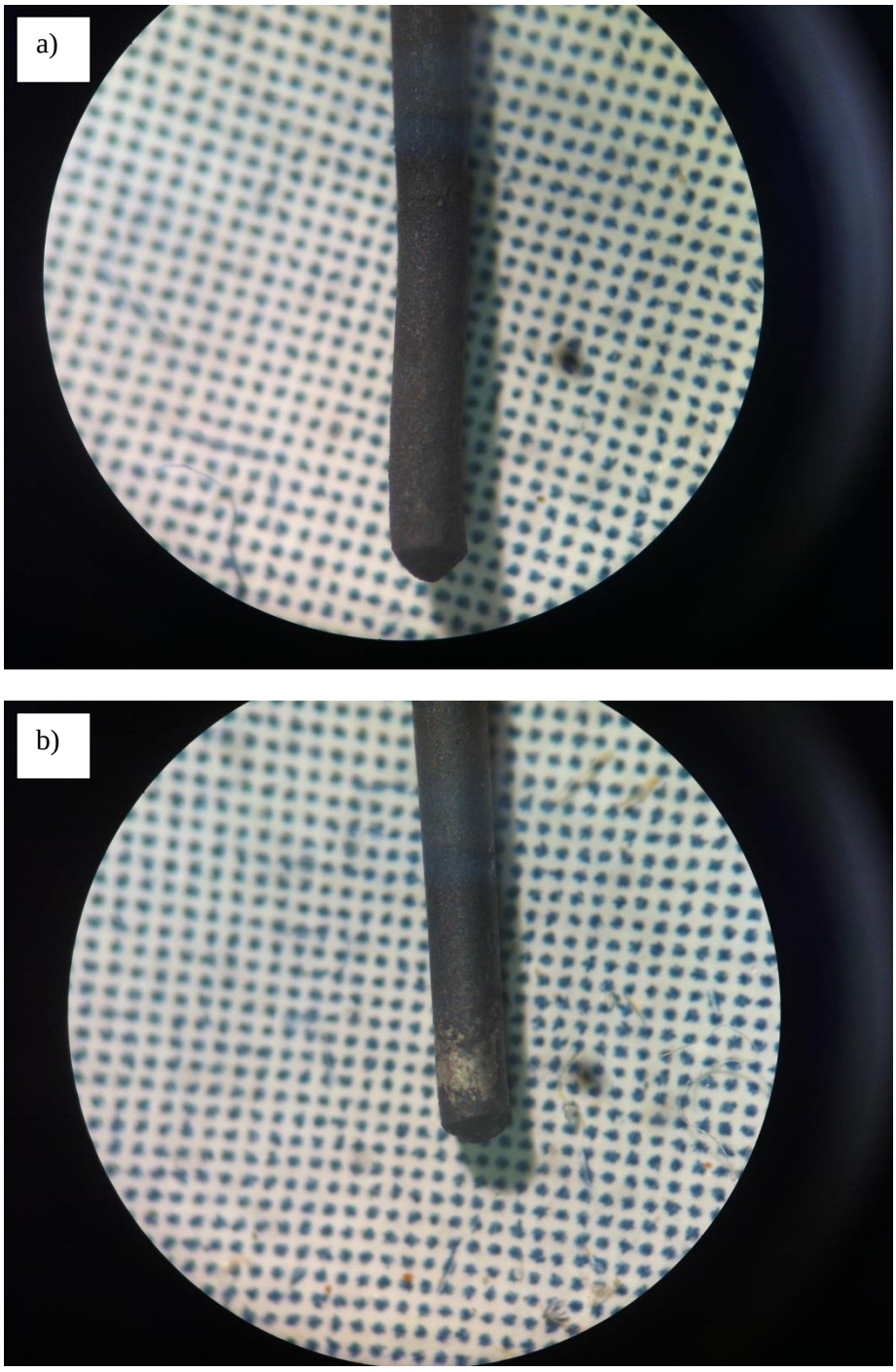

Figure 2- 8: Microscope observations of oxide formed on Palladium wires. Differences in the appearance of the oxide layer when heated at 800°C for 20 minutes (a) compare to wire heated at 750°C for 20 minutes (b). Heating cycles were performed in an oxygen purged oven.

The PdO pH sensor was set into a plastic screw and tapped into the Au plated Ni block to securely hold it during experiments. In this configuration the oxidized pH sensitive end of the wire was exposed directly above the Fh layer. Experiments which measured pH changes during the application of reductive potentials were performed in a beaker with the Fh layer deposited on a glass slide. The potentials measurements, indicative of pH changes, were measured against a saturated calomel electrode (SCE) in saturated KCl solution. Refer to Figure 2-9 for a schematic of the PdO configuration in the Au plated Ni WE.

2.6.2. Eh Measurements

The measurement of Eh was performed separately during the application of reductive potentials. These measurements were done with a platinum wire versus the same SCE electrode used for the pH measurements. The use of Pt wire for Eh measurements is commonly used in lituerature.[14] The Pt wire was oriented in the same configuration as the PdO wire, except it was placed on the other side of the Au plated Ni WE (refer to Figure 2-9).

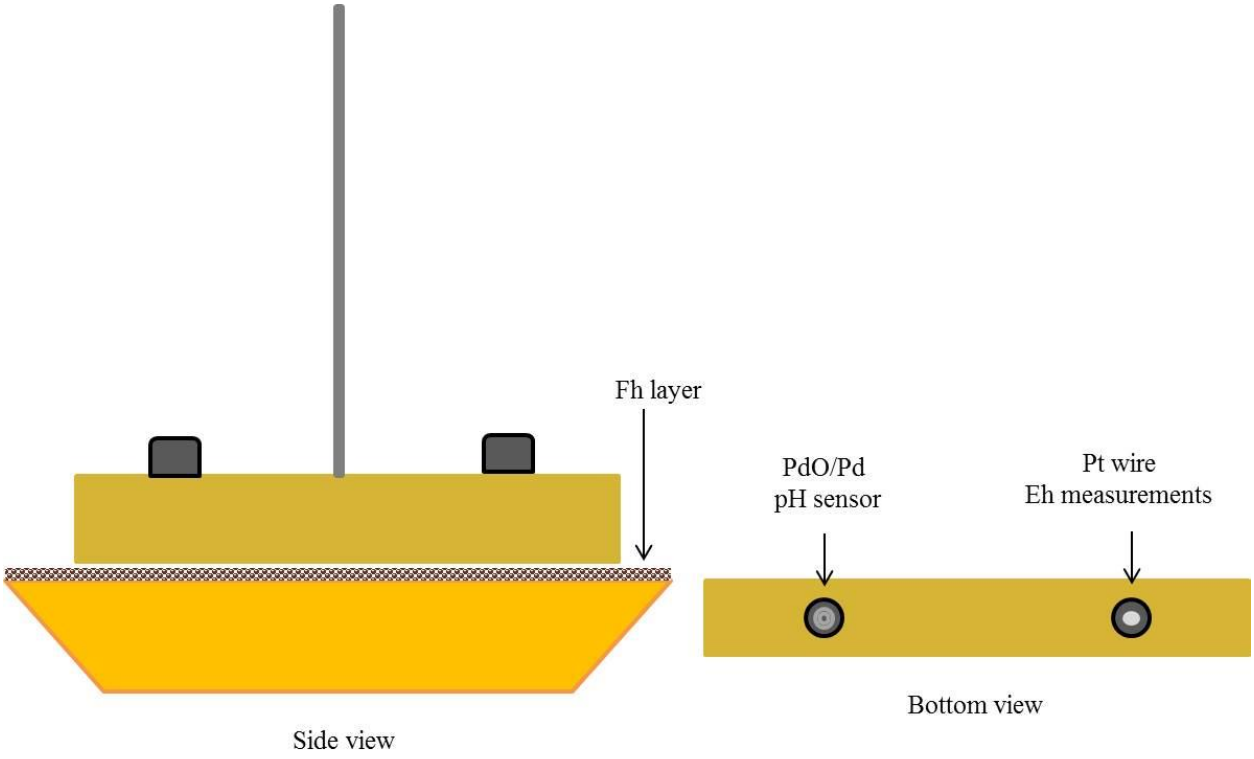

Figure 2- 9: Schematic of electrode orientation on the Fh covered ZnSe IRe for measurements of pH and Eh.

2.7.Reference List

1. Cornell, R. M.; Schwertmann, U. Synthesis. In *The Iron Oxides: Structure, Properties, Occurances and Uses*, WILEY-VCH: Weinheim, 2003; pp 525-540.
2. Jambor, J. L.; Dutrizac, J. E. *Chem. Rev.* **1998,** *98*, 2549-2585.
3. Parfitt, R. L.; Smart, R. St. C. *Soil Sci. Soc. Am. J.* **1978,** *42*, 48-50.
4. Parfitt, R. L.; Smart, R. St. C. *J. Chem. Soc. , Faraday Trans.* **1977,** *73*, 796-802.
5. Bhandari, N.; Hausner, D. B.; Kubicki, J. D.; Strongin, D. R. *Langmuir* **2010,** *26* , 16246-16253.
6. Das, S.; Hendry, M. J. *Chem. Geol.* **2011,** *290*, 101-108.
7. Pichler, T.; Hendry, M. J.; Hall, G. E. M. *Environ. Geol.* **2001,** *40*, 495-506.
8. Mazzetti, L.; Thistlethwaite, P. J. *J. Raman Spectrosc.* **2002,** *33*, 104-111.
9. Russell, J. D. *Clay Miner.* **1979,** *14*, 109-114.
10. Hiemstra, T.; Van Riemsdijk, W. H. *Geochim. Cosmochim. Acta* **2009,** *73*, 4423-4436.
11. Rosendahl, S. M.; Danger, B. R.; Vivek, J. P.; Burgess, I. J. *Langmuir* **2009,** *25*, 2241-2247.
12. Kohl, P. A. Electrodepostion of Gold. In *Modern Electroplating*, Fifth Edition ed.; Schlesinger, M., Paunovic, M., Eds.; John Wiley & Sons, Inc.: 2010; pp 115-130.
13. Grubb, W. T.; King, L. H. *Anal. Chem.* **1980,** *52*, 270-273.
14. Jones, C. A.; Langner, H. W.; Anderson, K.; McDermott, T. R.; Inskeep, W. P. *Soil Sci. Soc. Am. J.* **2000,** *64*, 600-608.

3. Results and Discussion

3.1. Electrochemistry

Electrochemistry was performed on ferrihydrite to indicate the potentials required to reduce Fe(III) within ferrihydrite. This was done by dropcasting a layer of Fh on the surface of the working electrode prior to the performance of cyclic voltammetry (CV). The reference used was a CV of the clean Ni disk WE in the absence of Fh which highlights that there are no redox reactions occurring in the potential range used for this experiment (dashed line in Figure 3-1). With the deposition of Fh on the surface of the WE (Figure 3-1, solid line) the first noticeable change was the increased current, caused by an increase in the double-layer capacitance compared to the clean Ni disk. The increased current that starts at ~-600 mV is an indication of the reduction of Fe(III) (refer to Figure 3-1). From this result it would be expected that the dissolution of Fh would start at ~-600 mV in the spectroelectrochemical experiments.

3.2. ATR-FTIR

3.2.1. Open Circuit Conditions

When there is no current flow in the ATR-FTIR cell it is considered to be at open circuit conditions. Experiments performed at open circuit potentials (OCP) were performed to determine the behaviour of arsenic adsorbed on ferrihydrite in the absence of an external electrical perturbation. These experiments proved to be able to differentiate between As(III) and As(V) adsorbed to the ferrihydrite surface.

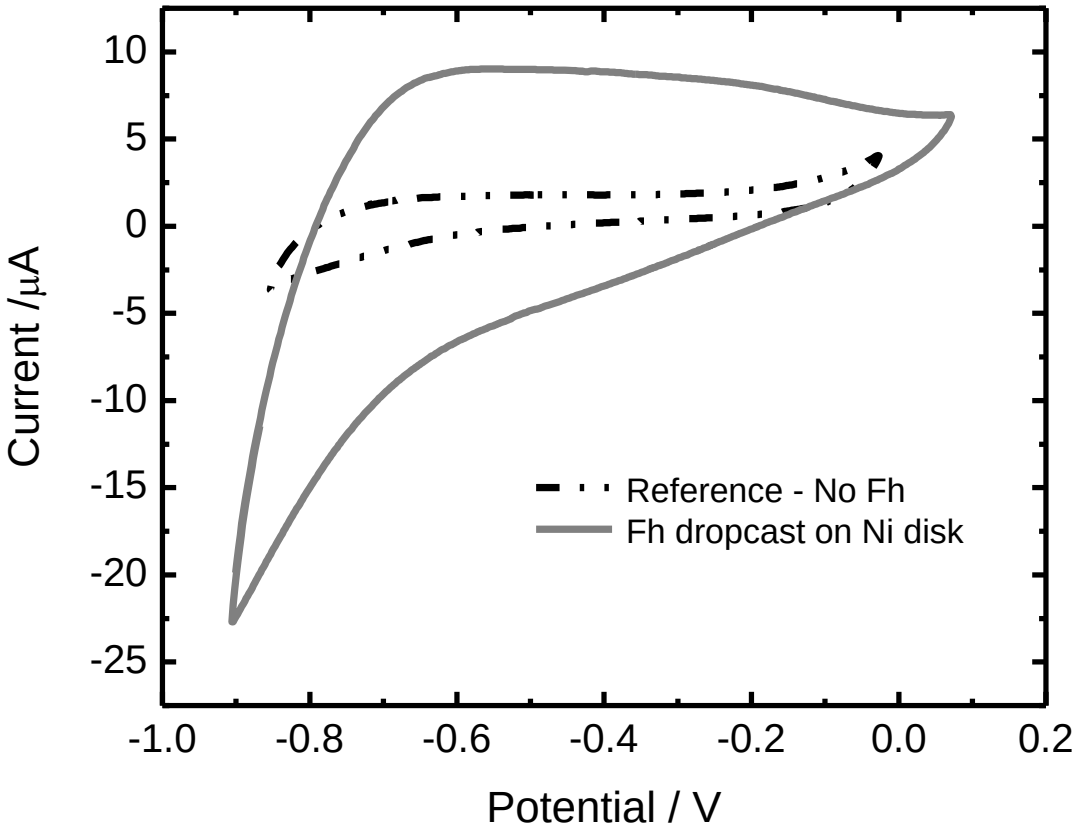

Figure 3- 1: Electrochemistry of Fh in 0.1 M KCl electrolyte, 50 mV/sec scan rate. Ni disk working electrode, Pt counter electrode, and Ag/AgCl reference electrode. 0.1 M KCl electrolyte.

3.2.1.1. As(III) on Ferrihydrite

Arsenite has relatively high pK_a values of 9.2 and 12.7 allowing for two available species at neutral pH; a totally protonated species, $As(OH)_3$, and a partially deprotonated species, $As(OH)_2^-$ (refer to Figure 1-1 for As(III) pH induced structural changes). The fully protonated species, $As(OH)_3$, with C_{3v} symmetry has two IR active modes, corresponding to E and A_1 modes. However, due to the low wavenumber cut-off of the ZnSe IRE used for these experiments we were unable to observe these vibrational modes. At high pH As(III) becomes partially deprotonated, this reduces its symmetry to C_s, $As(OH)_2O^-$. The reduction in symmetry splits the totally symmetric mode, E, into the symmetric (A') and asymmetric (A") vibrations.[1] The frequency for As-O undergoes a shift compared to As-OH which allows for observation above the ZnSe cut-off. Loss of the proton decreases the bond length of As-O compared to As-OH. The frequency shift to higher wavenumbers (centered on ~800 cm^{-1}) is attributed to the shorter stronger bond length.[2,3]

The discussion for the OCP experiments will be focused around three spectral regions; 650→900 cm^{-1}, 900→1200 cm^{-1}, and 1275→1575 cm^{-1}. These regions represent the adsorption of arsenite, desorption of sulfate, and the desorption of carbonate, respectively. As previously described, ATR-FTIR spectra are presented as a normalized comparison to a reference spectrum as ΔS/S (refer to *Experimental 2.2.2.3*). In this form, an increased surface concentration is observed as a negative absorbance while a positive absorbance represents a decreased surface concentration. See Figure 3-2 for the ATR-FTIR spectra of adsorbed As(III) on ferrihydrite. The first region of this spectrum (650→900 cm^{-1}) represents As(III) vibrations. The initial pH of this experiment was measured at 10.2 which, as previously described, allows for a partially deprotonated species, $As(OH)_2O^-$ in addition to $As(OH)_3$. This species gives rise to one observable band attributed to the As-O vibration, centered at 785 cm^{-1} (see Figure 3.2). These experiments were performed over long time periods to allow the adsorbed species to approach equilibrium. The integration of the time resolved data found that the adsorbed As(III) species essentially remains constant over the measured time (Figure 3-3). The As-O vibration maintains a constant peak

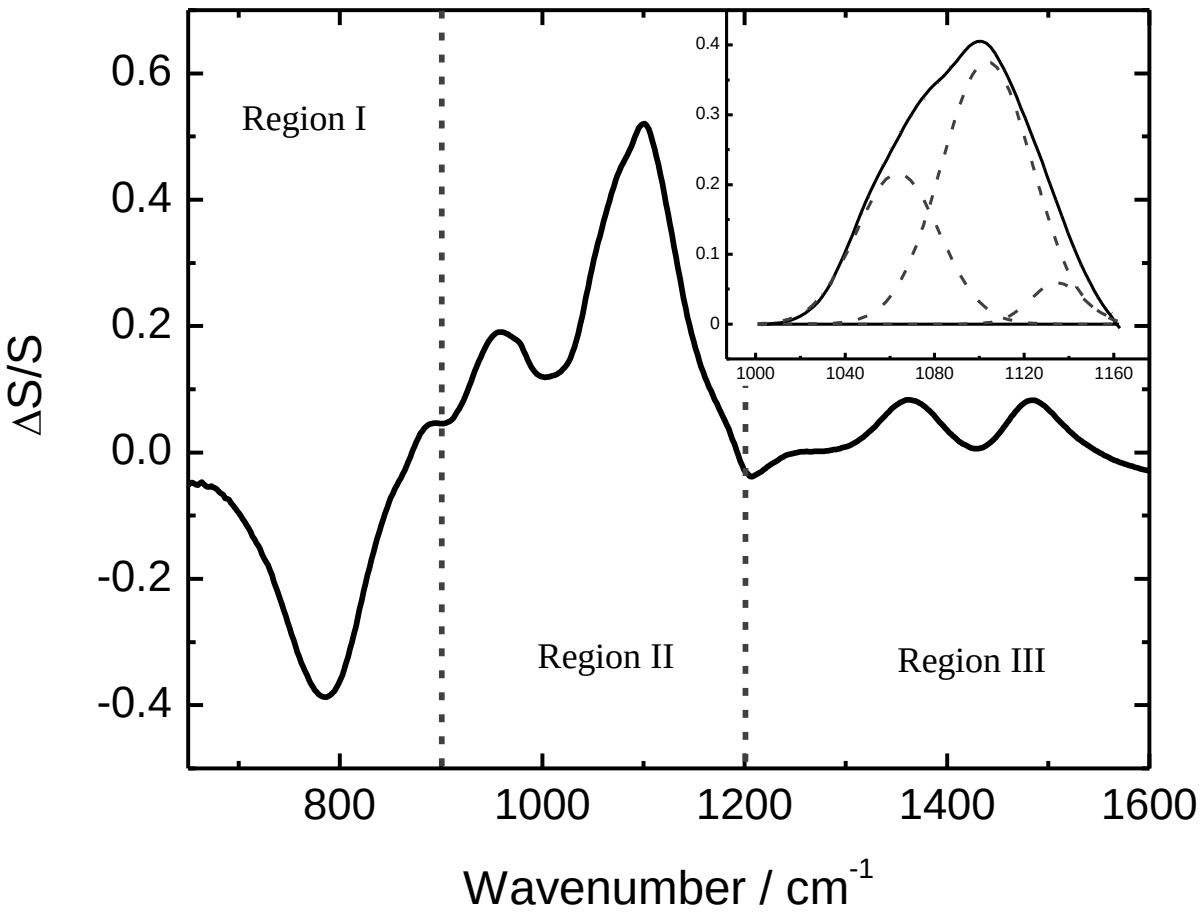

Figure 3- 2: 10 mM As(III) on Fh, 84 minutes after initial adsorption. Reference spectrum: Fh in D_2O; Sample spectrum: 84 minutes after the addition of 10 mM As(III). Inset: Deconvolution of sulfate adsorption showing three contributions to this feature.

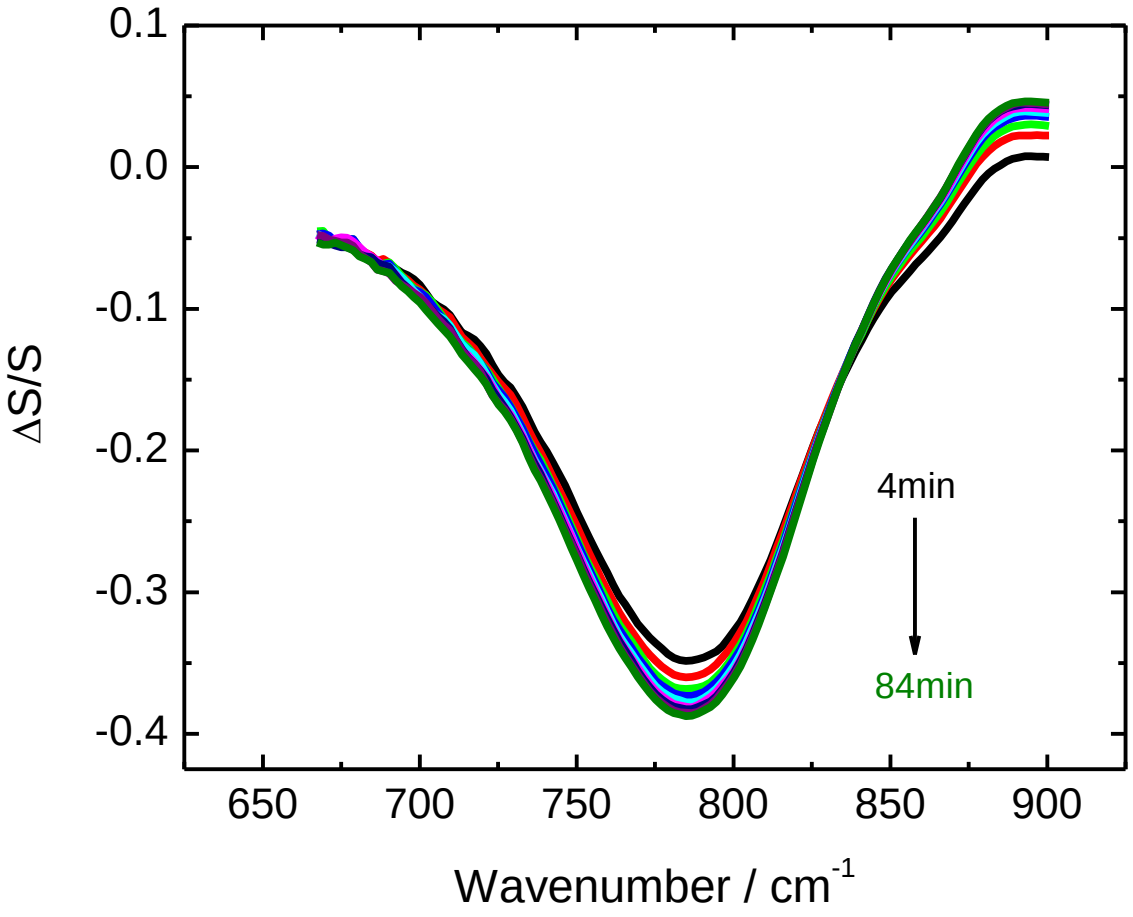

Figure 3- 3: Open circuit conditions of As(III) adsorption over 84minutes, measured at 10 minute intervals. Reference spectrum: Fh and D_2O; Sample spectrum: at corresponding time after addition of 10 mM As(III).

position and area, with only a slight increase in peak intensity. This indicates no substantial changes of adsorbed As(III) species, after the initial adsorption during the measured time period. Species which were previously adsorbed to the ferrihydrite are released due to the adsorption of As(III). This region of the spectra is also associated with carbonate vibrations.[4] These vibrations are found at ~880cm^{-1} for CO_3^{2-}•$6H_2O$ and ~840cm^{-1} from HCO_3^-•$6H_2O$ although, these modes are presumably insignificant due to their very low intensity relative to the strong As absorption in the same region.

The second region of interest (900→1200 cm^{-1}) has two main features centered at 960 cm^{-1} and 1100 cm^{-1} with contributions from D_2O and sulfate desorbing from the Fh surface. The presence of adsorbed sulfate can be explained by the synthesis method for Fh (refer to Figure 3-2, region II and inset). The feature at 960 cm^{-1} has two spectral contributions: Firstly a vibrational band from Fe-OD, caused by the deuteration of ferrihydrite surface hydroxyl groups, centered at 954 cm^{-1}.[4,5] Secondly, the appearance of a shoulder at higher wavenumber is a contribution from a sulfate vibration at 977 cm^{-1}. Sulfate has several vibrational contributions which change depending on adsorption configuration on the Fh surface. Consideration of the potential surface complexes should be discussed for insight into the sulfate vibrations. Two main types of surface complexes can form; outer-sphere and inner-sphere complexes. Outer-sphere complexes are a weak ionic interaction with the surface that can cause a slight distortion of the species symmetry, which can show slight changes in the IR active modes compared to the species in solution. Inner-sphere complexes are a direct bonding interaction with the Fh surface, which occurs by the replacement of FeOH and $FeOH_2^+$ surface sites, as discussed by Parfitt *et al*.[6,7] There are several configurations which are considered to be inner-sphere complexes (Figure 3-4b-d). The fitting of multiple Gaussian peaks to the feature at 1100 cm^{-1} was done in an attempt to determine the vibrations which contribute to this feature. Hug and Peak *et al*. have investigated this method of peak fitting for the deconvolution of sulfate adsorbed on iron(III) oxyhyrdoxides.[8,9] Gaussian peak fitting of the 1100cm^{-1} feature identified three components at 1055 cm^{-1}, 1101 cm^{-1}, and 1168 cm^{-1} (Figure 3-2 inset). These four vibrational modes indicate the presence of an inner-sphere complex although, the most intense vibration

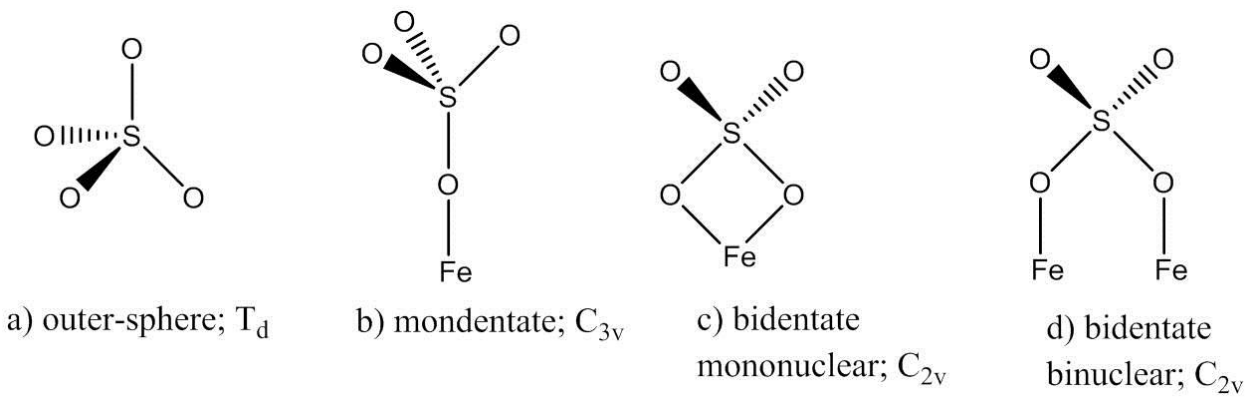

Figure 3- 4: Sulfate bonding complexes with point group symmetries.

is observed at 1101cm^{-1} which is attributed to asymmetric vibration of SO_4^{2-} with T_d symmetry. The additional contributions to this absorbance, at 1055cm^{-1} and 1168cm^{-1}, suggest the presence of an inner-sphere bidentate complex. The adsorption of sulfate to iron (III) oxy-hydroxides has been studied in-depth by both Hug and Peak *et al*.[8,9] These studies emphasize the four spectral components of adsorbed sulfate with C_{2v} symmetry. The normal modes of vibration for SO_4^{2-} with T_d symmetry are split due to a reduced symmetry of the bidentate inner-sphere complex. The bands observed in this study (Figure 3-2) suggest the major contribution of this absorbance is characteristic of SO_4^{2-} with distorted T_d symmetry in addition to a minor contribution from bidentate inner-sphere complex formation.

The final spectral region from 1275 to 1575 cm^{-1} (Figure 3-2, region III) is attributed to desorbing carbonate from the ferrihydrite surface. During the synthesis of Fh the pH is increased in open air conditions, this allows for the conversion of dissolved CO_2 to CO_3^{2-} which then adsorbs to the surface of the ferrihydrite. Carbonate is released from the surface during the adsorption of arsenic species. Studies performed by Su *et al.* show carbonate adsorbs to amorphous iron oxides in a monodentate complex with changes in the observed bands with changing pH and concentration.[10] They observed that at high pH the most intense ν_3 C-O symmetric and asymmetric vibrational bands are measured between 1474-1487 cm^{-1} and 1336-1359 cm^{-1} along with low intensity bands 950 cm^{-1} and 1070 cm^{-1}.[4,10,11] The bands observed in Figure 3-2, centered at 1362 cm^{-1} and 1486 cm^{-1} are in agreement with a monodentate complex with C_{2v} symmetry. The low intensity bands at 950 cm^{-1} and 1070 cm^{-1} are not observed in this study, most likely due to the overlap with the sulfate region.

3.2.1.2. As(V)

Arsenate has several available species; $As(OH)_3O$, $As(OH)_2O_2^-$, $As(OH)O_3^{2-}$, and AsO_4^{3-}, corresponding to pK_a values of 2.3, 6.8, 11.6 (refer to Figure 1-2 for structures changes of As(V) with changing pH). The totally deprotonated species has the highest symmetry, T_d, with one triply degenerate IR active mode of T_2. Decreasing pH increases the protonation of the As(V) species, which also

decreases the symmetry. For $As(OH)_3O$ and $As(OH)O_3^{2-}$ with C_{3v} symmetry the triply degenerate mode splits into A_1 and 2E IR active vibrational modes. An additional loss of symmetry to C_{2v} for the $As(OH)_2O_2^-$ species splits the doubly degenerate E mode which gives rise to B_1 and B_2 vibrational modes in addition to the A_1 mode. Goldberg *et al*. have performed in depth studies on the adsorption of arsenic species to oxides.[2] These studies have observed a splitting of the As-O vibration due to surface coordination. Specific to iron oxide coordination Goldberg determined a vibration at 817-824 cm^{-1} corresponding to As-O-Fe and a vibration at 854-861 cm^{-1} corresponding to a non-coordinate As-O vibration.[2]

Initial As(V) experiments were performed in the absence of Fh to determine the behaviour of it in solution. Figure 3-5 illustrates the ATR-FTIR spectra for As(V) in solution at pH 5, 8.5, and 12, with corresponding dominant species of $As(OH)_2O_2^-$, $As(OH)O_3^{2-}$, and AsO_4^{3-} respectively. At pH 5 the dominant species in solution is $As(OH)_2O_2^-$, which has two IR active modes for the symmetric and asymmetric As-O stretches at 878 cm^{-1} and 907 cm^{-1} (refer to Figure 3-5, bottom spectrum).[2] At pH 8.5 the As(V) species is partially deprotonated to $As(OH)O_3^{2-}$, which gives rise to a signature vibrational band at 855 cm^{-1}, that is in agreement with the asymmetric As-O stretch given by Goldberg and others (Figure 3-5, middle spectra).[1,2] At pH 8.5 several experiments were performed with increasing As(V) concentration which increases the intensity of the As-O feature. At pH 12 an additional band is observed at 803 cm^{-1}, which is assigned to a totally deprotonated species, AsO_4^{3-} (Figure 3-5, top spectrum), in addition to the As-O vibration at 855 cm^{-1} assigned to $As(OH)O_3^{2-}$.[11,12] As previously stated the stretching vibration assigned to As-OH vibration is below the cut-off of ZnSe IRE and therefore not observed in this study.

Figure 3-6 illustrates the spectra obtained due to As(V) adsorption on ferrihydrite. Features observed above 900 cm^{-1}, attributed to sulfate and carbonate desorption, will not be discussed in this section (see section *3.2.11 As(III) on Ferrihydrite*). As(V) adsorption is centered at 836 cm^{-1} with a non-Gaussian line shape when compared to As(V) in solution. This indicates the presence of more than one

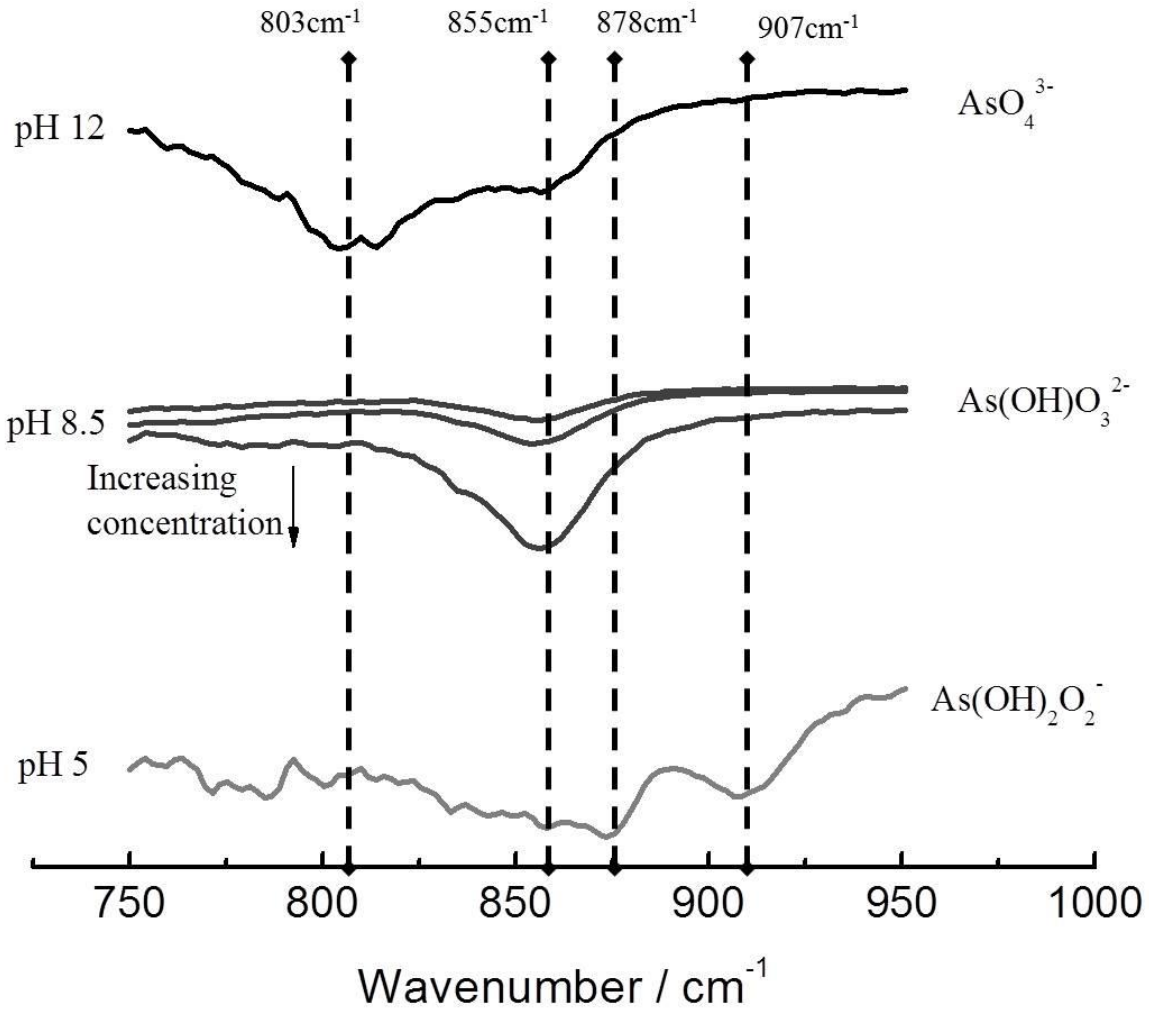

Figure 3- 5: As(V) in solution (no Fh). Reference spectra: D_2O on Ge IRE; Sample Spectra: As(V) adjusted to corresponding pH.

Top Spectra: pH increased to 12 with NaOD solution introducing an AsO_4^{3-} species with observed band at 803 cm^{-1} (top spectra).

Middle Spectra: Natural pH at 8.5 with dominant $As(OH)O_3^{2-}$ species with spectral feature at ~850 cm^{-1}, increased concentrations given increase intensities.

Bottom Spectra: pH decreased with HCl diluted in D_2O introduces a dominant feature at 878 cm^{-1} and 907 cm^{-1} for an $As(OH)_2O_2^-$.

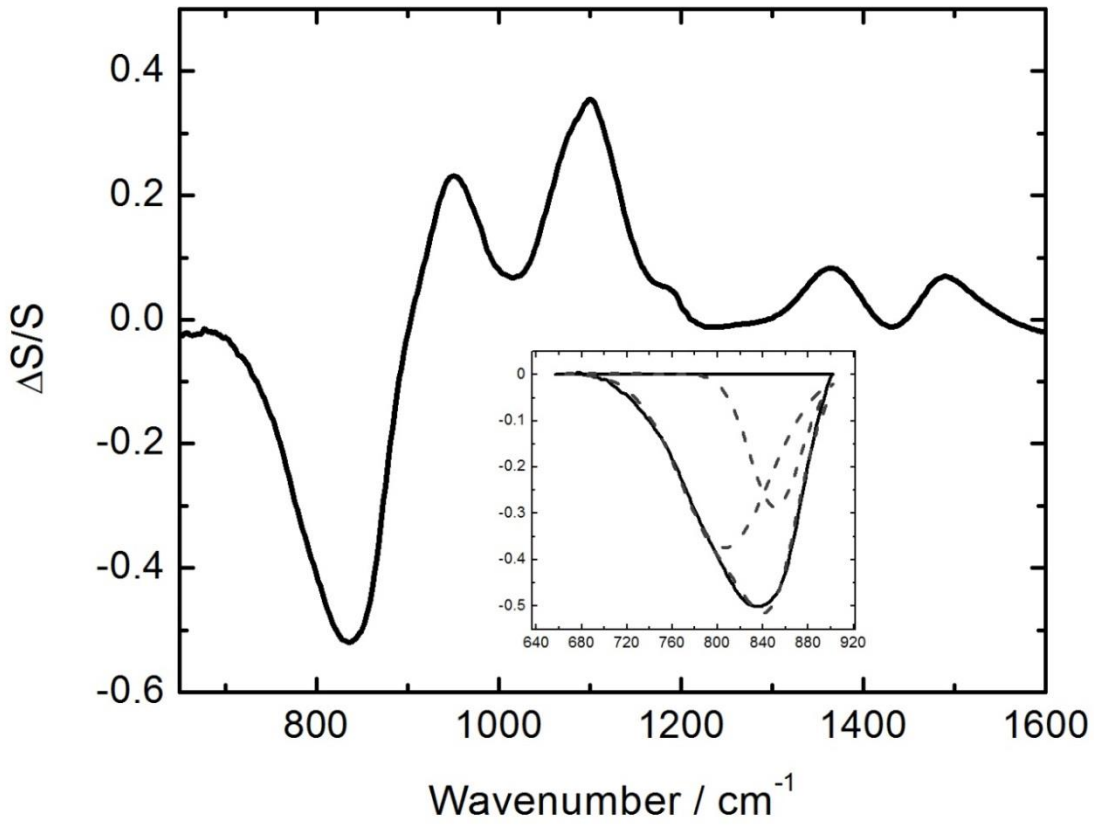

Figure 3- 6: As(V) adsorbed on Fh. Reference spectra: D_2O Fh on ZnSe IRE; Sample Spectra: 84 minutes after the addition of 10 mM As(V). Inset: deconvolution of As(V) vibrations to highlight contributions at 804 cm^{-1} (Fe-coordinate) and ~845 cm^{-1} (non-coordinate).

spectral component in the 836 cm^{-1} feature. The pH was measured to be 8.8 indicating that the dominant species was $As(OH)O_3^{2-}$. In an effort to resolve the features contributing to the 836 cm^{-1} absorption, multiple Gaussian peaks were fit to the feature. The Gaussian peak fitting gave rise to two contributing features at 804 cm^{-1} and 847 cm^{-1} (refer to inset in Figure 3-6). Upon investigation of the literature, these peaks are attributed to As-O-Fe vibration and non-coordinate As-O vibration (Figure 3-7).[2,13] The resolution of two features indicates the formation of inner-sphere complexes with the Fh surface. Time resolved data of the Gaussian peak fits was used to observe changes as the system approaches equilibrium. In interpretation of the time resolved data the introduction of an additional species would appear in one of two ways. First, a shift in peak position would indicate change in the As-O species, and second an increase in the width of the peak would indicate the appearance of an additional As-O species. Limited change is observed in the peak widths (Figure 3-8c) and the peak centers (Figure 3-8b) indicating the nature of the adsorbed species remains constant throughout the measured time period. Observation of the peak intensity (Figure 3-8a) and peak area (Figure 3-8d) give rise to an independent relationship between the Fe-coordinate and non-coordinate As-O vibrations. The non-coordinate species, centered at 847 cm^{-1}, has limited changes over the 84 minute time period. In contrast the Fe-coordinate species, located at 805 cm^{-1}, has an increased peak area and intensity (note: due to negative nature of this band an increased intensity is observed as more negative). This indicates that the total surface coverage of Fh by As(V) species increases over time. The initial adsorption of As(V) occurs quickly and slowly increases until ~75 minutes when it starts to approaches an equilibrium of surface coverage.

3.2.2. Spectroelectrochemistry

The focus of this thesis was to use electrochemistry as a means to expose ferrihydrite adsorbed arsenic species to reductive conditions and determine the changes in the adsorbed complexes, desorption of As(V) and As(III), and dissolution of Fh. Spectroelectrochemistry was used to perform *in-situ* experiments to relate solution potential to the adsorbed species on the Fh surface. In addition to the changes to adsorbed species these experiments were performed on Fh alone to determine the changes in

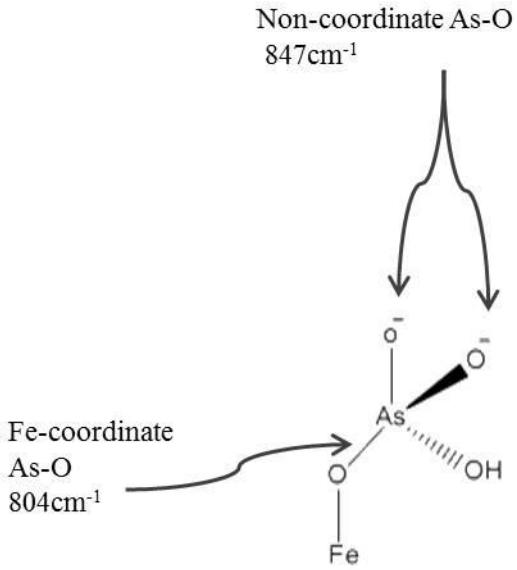

Figure 3- 7: As-O and Fe-O-As IR contribution from adsorbed As(V).

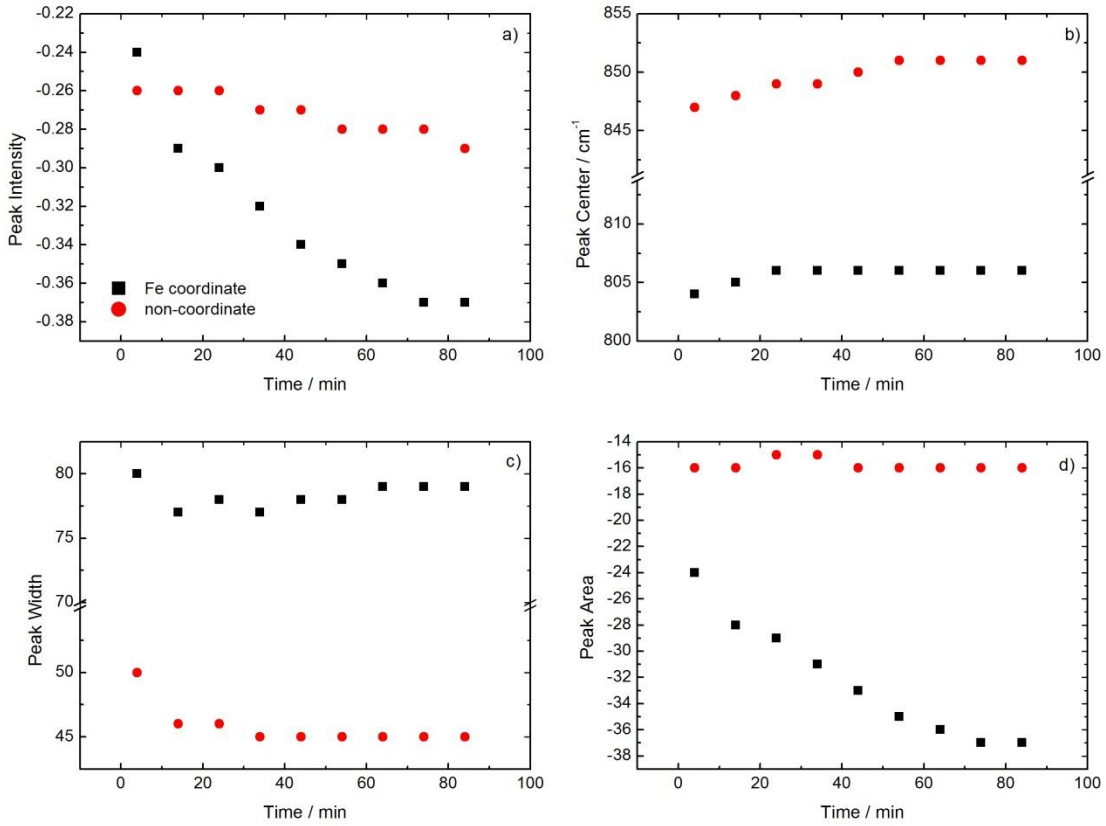

Figure 3- 8: OCP As(V) on Fh function of time data. Time resolved data highlights the changes in the As-OFe (coordinate) and As-O (non-coordinate) through investigation of peak intensity (a), shift in peak center (b), peak width (c), and total peak area (d).

the Fh under reductive conditions.

3.2.2.1. Ferrihydrite

In order to understand the behaviour of Fh under reductive conditions several experiments were performed in the absence of adsorbed arsenic. The IR active band of Fh is observable at ~700 cm^{-1}. Ferrihydrite is known to have limited stability and undergo transformations to goethite (α-FeOOH) and hematite (α-Fe_2O_3) due to temperature increases and acidic or basic conditions. Figure 3-9 illustrates the implication of reductive potentials to the Fh surface. The high intensity feature centered at 970 cm^{-1} and 1100 cm^{-1} is due to the release of surface adsorbed sulfate. This process is presumed to be concomitant with Fh dissolution or phase changes in the mineral phase. Two features between 1300 and 1600 cm^{-1} are attributed to desorption of carbonate on the Fh surface. Features observed at ~890 cm^{-1} are assigned to an additional band from adsorbed CO_3^{2-}, this feature is not observed at OCPs (see Figures 3-2 and 3-6) presumably due to overlap with the As(III) and As(V) features.[14] Changes in the Fe-OD is also observed at ~950 cm^{-1} (previously discussed in section *3.2.1.1. As(III) on Ferrihydrite*).[5] At potentials of ~-700 mV (with Au WE) the reduction of neutral water is expected, which in turn will increase the pH of the solution due to the generation of OH^- (see section 3.2.2.2 for further discussion on this topic). Desorption of sulfate and carbonate in part may be attributed to competitive adsorption of OH^- to the Fh surface. At low wavenumbers (~700 cm^{-1}) a positive band is observed at increasingly negative potential application. At these negative potentials it is expected that Fh may undergo a phase transformation. Das *et al.* determined the transformation of Fh to goethite (α-FeOOH) and hematite (α-Fe_2O_3) occurs due to elevated temperature and pH on the order of a day, while at room temperature only a 10 % transformation occurred after a couple of weeks.[15] It is most likely that the low wavenumber feature in Figure 3-9 is due to a loss of the characteristic Fh IR vibration due to phase transformation. As stated, Das *et al.* observed Fh transformation to be on the order of a day. Considering the short time periods of these experiments (~15 minutes) the total transformation of Fh would not be expected. A phase transformation of Fh should result in additional observed bands in the ATR-FTIR spectra, although no new bands are observed. A

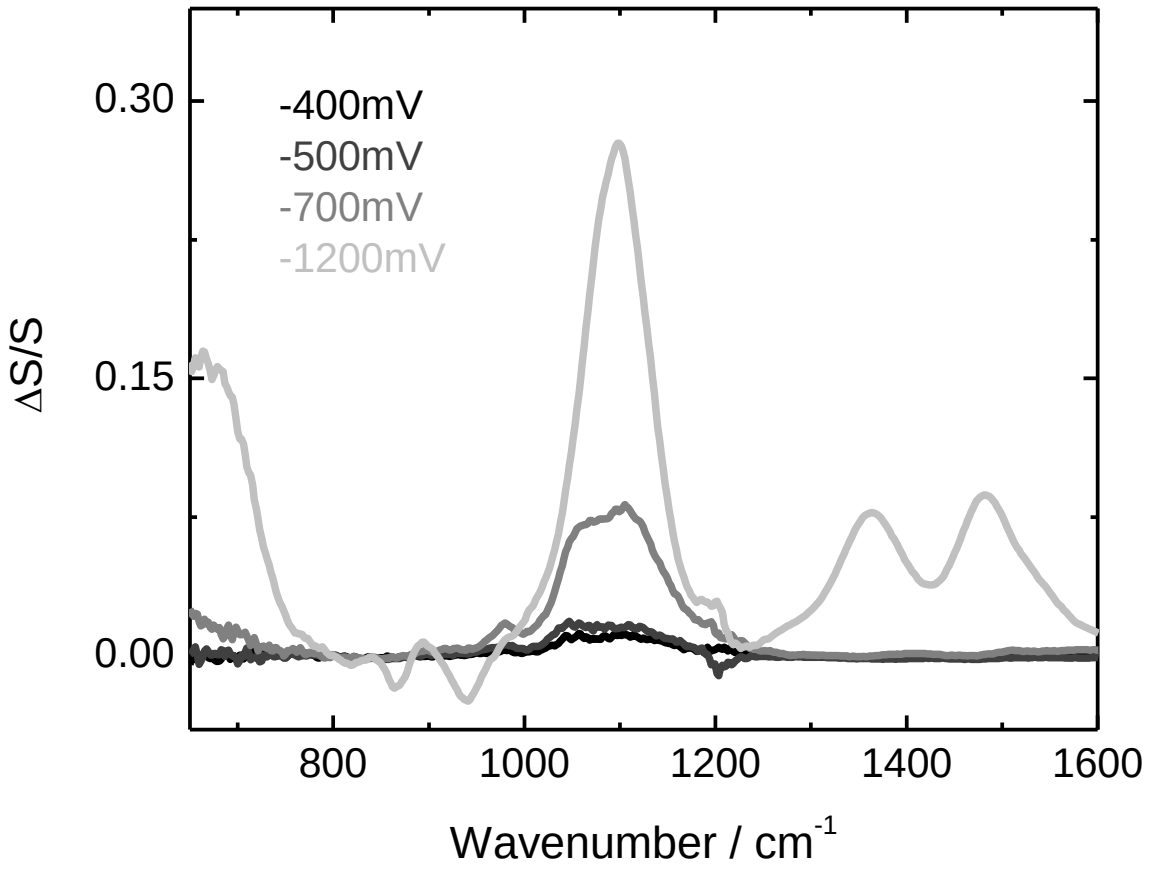

Figure 3- 9: Spectroelectrochemical changes to Fh after 15 minutes of each applied potential. Reference spectra: measured immediately before the application of the potential.

plausible explanation for this is that characteristic vibrational bands for α-FeOOH and α-Fe_2O_3 are observed at 297, 384 cm^{-1} for goethite and 222, and 290 cm^{-1} for hematite but due to the IR cut-off of ZnSe these bands are not observable in this study.

3.2.2.2. As(III) on Ferrihydrite

Several studies, performed by Tufano *et al*., have used iron-reducing bacteria, specifically *Shewanella putrefaciens*, as a method to study desorption of arsenite from ferrihydrite.[16,17] These studies have associated the desorption of As(III) from ferrihydrite with the reduction of Fe(III) to Fe(II). This dissolution is attributed to the release of the bound As(III) from the surface. They also found the dissolution of iron to be an intermediate stage in the phase change of ferrihydrite to goethite or hematite, which upon formation allows for the re-adsorption of As(III) to the new mineral phase. The use of bacteria by many researchers has found that reductive conditions contribute to the release of adsorbed As(III) species from Fh. This thesis uses *in-situ* spectroelectrochemistry as an additional approach to measure the effects of reductive conditions on Fh adsorbed As(III). Electrochemistry presents an appealing method to control the reductive conditions effecting As(V) on Fh in conjunction with ATR-FTIR to measure the changes during potential application.

Figure 3-10 illustrates the results from the spectroelectrochemical experiment performed on arsenite adsorbed to ferrihydrite with an initial pH of 10.2. These experiments show that under mildly reductive conditions, -150mV, -300mV, and -600mV applied potential, there are no measureable changes in the As(III) or the Fh (Figure 3-10). It is only at more negative potentials that the release of As(III) from the surface is observed, through the appearance of an upward band at ~793 cm^{-1}. The consideration of several aspects should be discussed in order to understand the reason for which the As(III) is desorbing. As previously stated Tufano *et al.* associated the desorption of As(III) to be due to the dissolution of Fe(III) to Fe(II). Although this is a plausible explanation in these conditions it is unlikely for several reasons. First, the experimental changes determined by Tufano *et al.* were measured over days

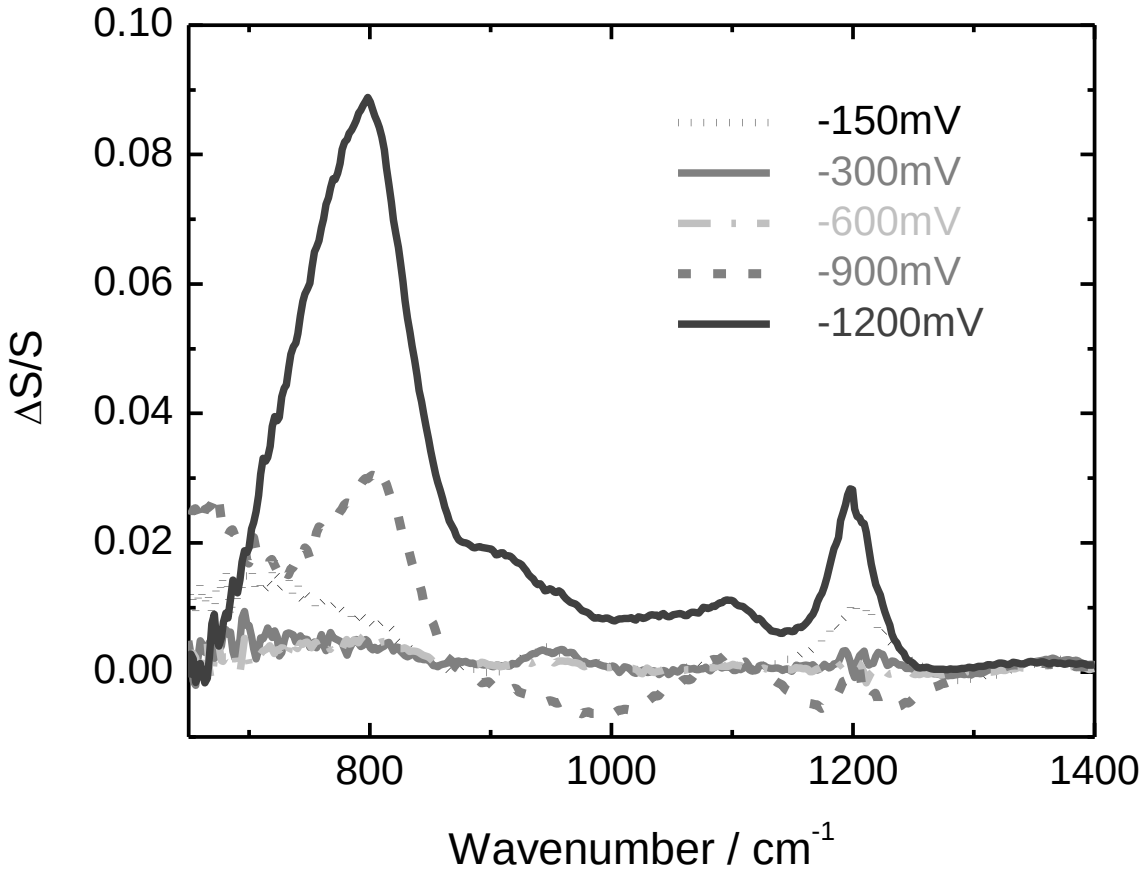

Figure 3- 10: As(III) on Fh spectroelectrochemistry. Reference spectrum: measured immediately before the application of the corresponding potential; Sample Spectra: measured after the potential had been applied for 15 minutes.

to weeks; the experiments performed in this body of work were performed over ~15 minutes. Also, a change in the iron(III) (oxy)hydroxide phase should be indicated with a loss of the signature Fh band centered at 700 cm^{-1}, which does not appear in these experiments (Figure 3-10). For this reason it is unlikely that ferrihydrite is undergoing a substantial phase transformation during the time period of these experiments. A more likely cause of the As(III) desorption is the increased pH, caused by the electrochemical reduction of water.[18]

$$2H_2O + 2e^- \rightarrow H_2 + 2OH^- \qquad (3\text{-}1)$$

The pH change can be estimated, assuming the current that is generated is strictly for water reduction (reaction 3-1). The steady-state current that was measured during the application of -1200 mV for ~20 minutes was found to be -455 µA. The information in the following calculation can be used as a gross approximation of the pH change:

$$455\ \mu A \times 1430\ sec = 0.65\ C \times \frac{mol\ e^-}{96485\ C} \times \frac{2\ mol\ OH^-}{2\ mol\ e^-} = 6.7x10^{-6}\ mol\ OH^-$$

The volume of solution between the WE bar and the Fh surface can be assumed to be defined by a ~50 µm cavity thickness (refer to Figure 2.7 for cell configuration):

$$0.6\ cm \times 5\ cm \times 5.0x10^{-3}\ cm = 0.015\ cm^3 = 1.5x10^{-5}\ L$$

Assuming that there was 10^{-7} M OH^- present prior to the application of the potential and that the generated OH^- moles remain in the small cavity below the working electrode the pH will increase substantially:

$$\frac{6.7x10^{-6} mol\ OH^-}{1.5x10^{-5}\ L} = 0.44\ M\ OH^-$$

$$pOH = -\log(0.44\ M\ OH^-) = 0.35$$

$$pH = 13.6$$

The above calculations give an idea of the pH increase that can be observed due to water reduction only at

100 % current efficiency. The current efficiency is limited by many experimental parameters including electrode orientation, diffusion, side reactions, as well as temperature and pressure.[19-21] In practice, diffusion controlled mass transport will remove the electrogenerated OH^- from the cavity rather efficiently and the measured pH will presumably be more acidic then the value arrived at above. This type of estimation is difficult due to the number of assumptions that are required but nevertheless illustrates how a pronounced pH change can result from Equation 3-1. This approximation also illustrates the importance of finding a means to actually measure the pH in the thin cavity during electrolysis. Thus, due to the application of very negative potentials the desorption of As(III) is likely caused by competitive adsorption conditions where OH^- will adsorb to Fh. As illustrated in Figure 3-10 the release of As(III) from the Fh surface is achieved only at very reductive conditions when the generation of OH^- increases, and limited changes are observed at mildly reduction conditions.

3.2.2.3. As(V) on Ferrihydrite

A substantial number of studies surround the adsorption and desorption of arsenate to several different oxide layers.[22-24] The investigation of reductive conditions and its effects on the adsorption of arsenic species to iron(III) (oxy)hydroxides are normally achieved using microbial reduction.[16,25] Langner and Inskeep used a glucose-fermenting *Clostridium sp.* microbe for the reduction of As(V), finding this microbe is capable of reducing aqueous As(V) to As(III).[25] However, with As(V) adsorbed to an iron oxide surface they were unable to measure an increase in aqueous As species, indicating that the release of As from the surface is not significant in a 24 hour period.[25] Their study indicates that the reduction of As species has a limiting effect on the overall desorption of the species from iron oxide surfaces. Tufano *et al.* used two different strains of *Shewanella sp.*; ARM1 for the reduction of arsenic, and FERM for the reduction of iron.[16] This gave them the capability to isolate the cause of As desorption to be due to As(V) and/or Fe(III) reduction. This study was done over longer time periods compared to the previous study and determined that the reduction of As(V) allows for desorption from Fh. Although the reduction of Fe(III) alone or both As(V) and Fe(III) reduction actually inhibits the release of As due to

the precipitation of the dissolved iron into a new mineral phase which reabsorbs the As species.[16] Spectroelectrochemical experiments allow for more precise control of the system's potential allowing for a greater understanding of the conditions where arsenic will remain adsorbed to Fh. It was expected that with the application of reductive potentials arsenate will desorb from the Fh surface.

Several reductive potentials were used to determine the behaviour of Fh adsorbed As(V). These results are summarized in Figure 3-11. The initial potential applied was -50 mV which showed little to no changes in the adsorbed species. As previously discussed, at pH 8 and open circuit conditions, As(V) is predominately present as $As(OH)O_3^{2-}$ and has its main feature centered at 836 cm^{-1}. This can be deconvolved to give rise to two contributions, one at 804 cm^{-1} (Fe-coordinated) and another at 847 cm^{-1} (non-coordinate). Under the application of -200 mV there is an increase in adsorbed species, indicated by a negative band (Figure 3-11, red line). This feature is a broad low intensity peak that appears to have features at 830 cm^{-1} and 878 cm^{-1}. As discussed in the previous section, $As(OH)O_3^{2-}$ has a main feature centered at 836 cm^{-1} with two components at 804 cm^{-1} and 847 cm^{-1} attributed to Fe-coordinate and non-coordinate As-O vibration. This is most likely the contribution at 830 cm^{-1}, indicating an increase in the adsorbed species. The feature centered at 878 cm^{-1} is assigned to $As(OH)_2O_2^-$. This assignment warrants some investigation for its presence.[2] One possibility is electric field driven protonation effects caused during the application of reductive potentials.[26] Presumably this could increase the concentration of $As(OH)_2O_2^-$ at an applied potential of -200 mV. The application of -600 mV shows no new species being adsorbed or desorbed, although, at -800 mV desorption of $As(OH)_2O_2^-$ is observed with a positive band at 878 cm^{-1} (Figure 3-11). The most reductive potential used was -1200 mV, giving rise to desorption of $As(OH)O_3^{2-}$ feature at ~840 cm^{-1}. An additional feature is observed as a negative band centered at 803 cm^{-1}. Two possible assignments are found for this position: First, As(III) species, and second, a totally deprotonated arsenate, AsO_4^{3-}.[11,12,27] Kinetics must be considered in the assignment of this feature. The time required in the reduction of As(V)→As(III) is much longer than required for deprotonation of arsenate.[27] Slow kinetics is related to material used for the WE, in this case Au plated Ni, and the slow

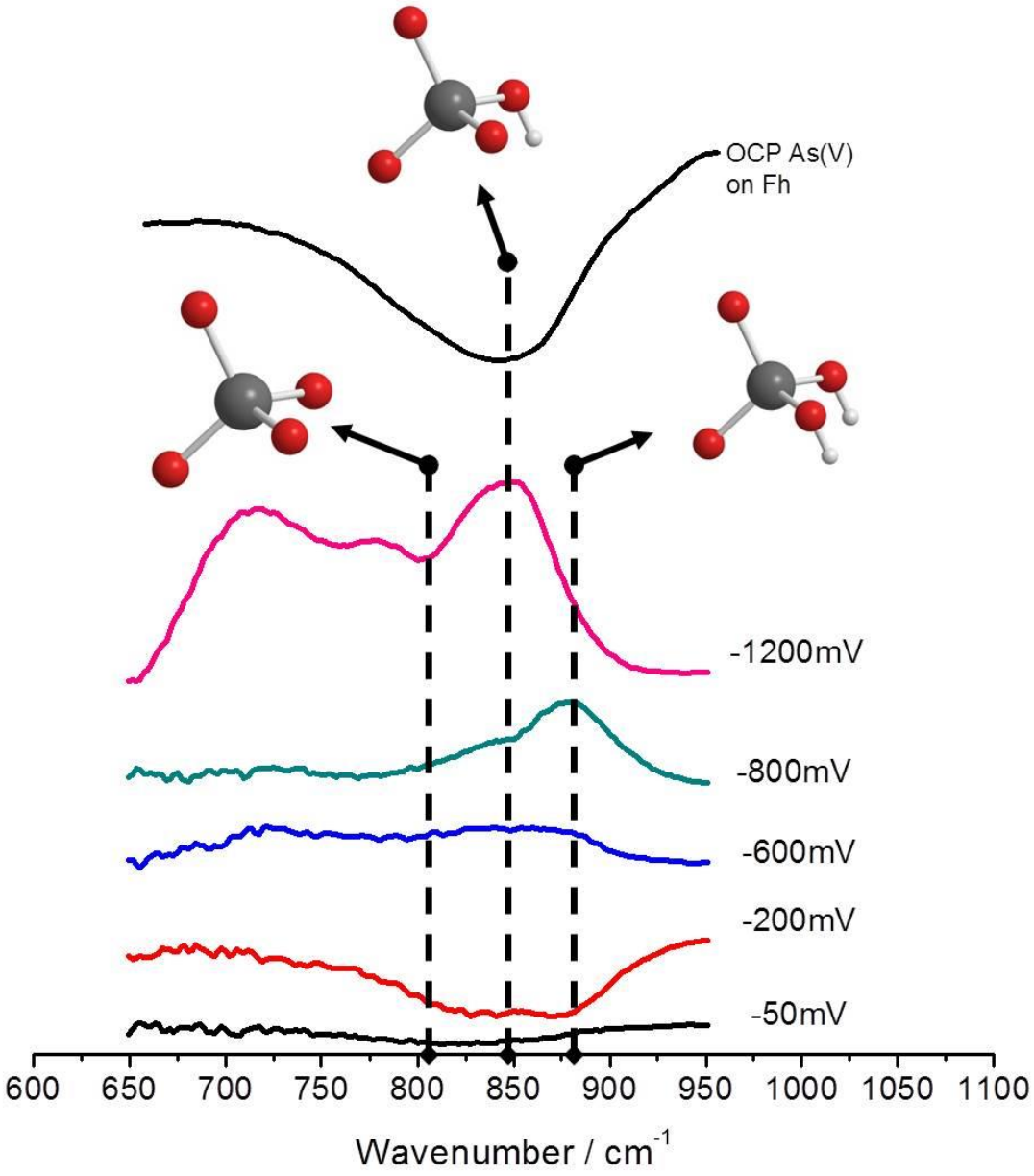

Figure 3- 11: As(V) on Fh spectroelectrochemical changes at different potentials compared to OCP measurements (top solid black spectra). Reference spectra: measured immediately prior to the application to the corresponding potential; sample spectra measured after 15 minutes of the corresponding applied potential.

heterogeneous electron transfer constants that are associated with As(V) reduction to As(III) on non-platinum electrodes.[28] Considering that the time scale of these experiments is relatively short, ~20 minutes of applied potential, it is most likely that this feature is a contribution from a totally deprotonated form of arsenate. An additional feature at low wavenumbers is most likely a contribution from the loss of Fh. At these reductive potentials it is most likely that Fh will start to reduce Fe(III) →Fe(II), Fe(II) which is a more soluble form of iron. As previously discussed the changes which are occurring are most likely caused by the increased pH, due to the generation of OH^- from the reduction of water at these negative potentials. Many studies have shown that at high pH (>pH 9) the adsorption of arsenate is diminished.[23] Presumably an increase to above pH 9 is possible for these experiments at such negative potentials. Initial experiments to investigate the effect of pH were completed at atmospheric conditions and manually increasing the pH (i.e. through titration experiments).

3.3. pH measurements

3.3.1. ATR-FTIR pH Titration

Titration experiments were performed to understand the changes in the adsorption and desorption behavior of arsenic species on ferrihydrite. These experiments were performed by manually increasing the pH of the solution.

As with previous experiments, initial experiments were performed on ferrihydrite with no adsorbed arsenic species. Figure 3-12 depicts the results from these experiments. As with the spectroelectrochemical experiments the most intense feature is due to the desorption of sulfate, centered at ~1100 cm^{-1}, along with changes in the carbonate adsorption at higher wavenumbers. The pH increase was done with a solution of 0.01 M NaOD. The Fe-OD vibration is present at ~950 cm^{-1} which is shown as an increased absorption. An additional low intensity band is observed at lower wavenumbers, ~840

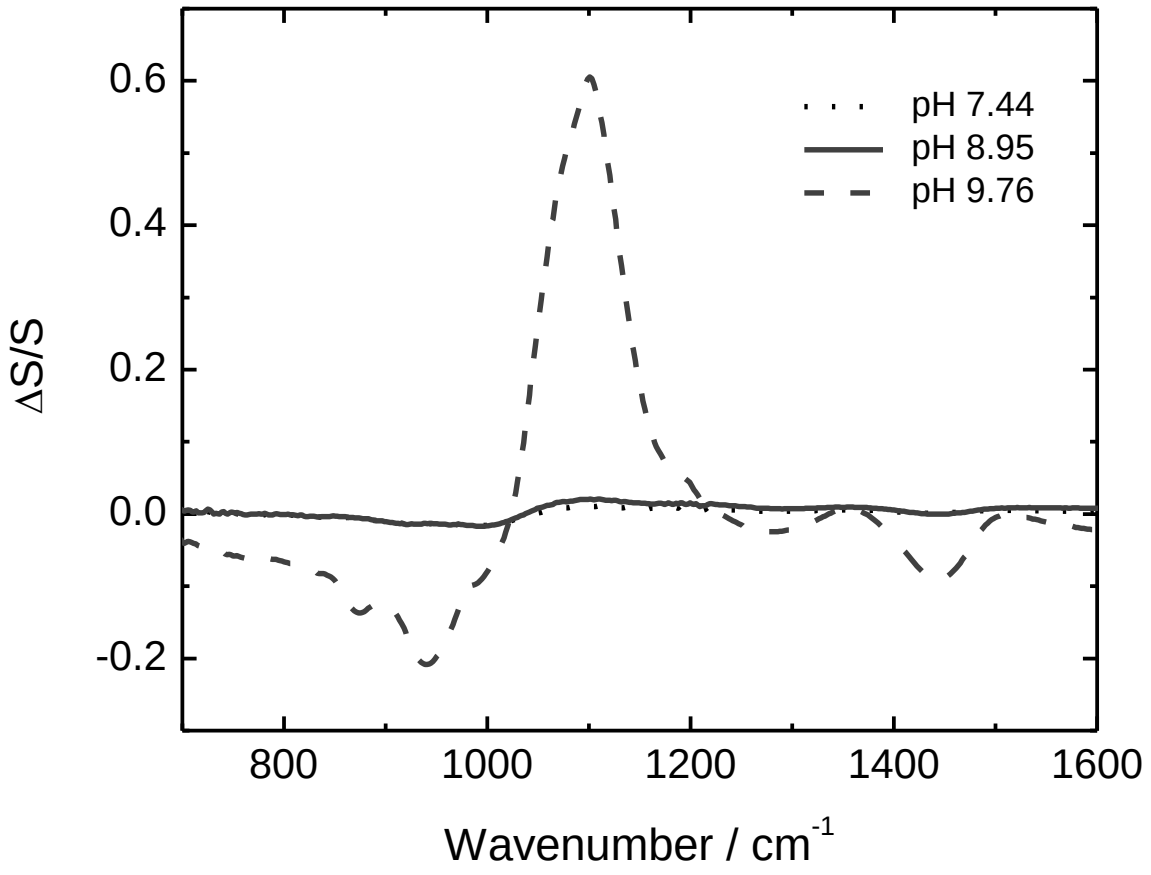

Figure 3- 12: Manual pH increase to Fh using 0.011 M NaOD solution. Reference spectra: Fh on ZnSe at natural pH ~7.4; Sample Spectra: after adjustment of pH.

cm^{-1}, which is most likely attributed to a CO_3^{2-} vibration from $CO_3^{2-} \bullet 6H_2O$.[4]

Changes in adsorbed As(III) species due to increasing pH are depicted in Figure 3-13. The loss of As(III) species, ~800 cm^{-1}, are observed as the pH approaches 11. As the second pK_a for arsenite is 12.7, it is unlikely that the pH is increased enough for the loss of an additional proton, although it seems there may be a decrease in the As-O bond length. As previously discussed, the observation of the As-O vibration is allowed due to the shorter bond compared to the As-OH bond. Previous OCP experiments observe the As-O vibration at ~790 cm^{-1} and these experiments show a similar band at only slightly higher wavenumbers. Presumably this change is due to a slightly higher pH which decreases the As-O bond, shifting the vibration to a slightly higher wavenumber. Increasing the pH in open air conditions also increases the adsorbed carbonate species, observed at 1450 cm^{-1}.

Increasing pH in the presence of As(V) adsorbed to Fh indicates that initially there is $As(OH)_2O_2^-$ present, with a characteristic band at ~880 cm^{-1} (see Figure 3-14). Presumably this is only a minor component to the As species present, as with a starting pH at ~8 the dominant species should be $As(OH)O_3^{2-}$. As the pH increases, the vibration from desorbed $As(OH)_2O_2^{2-}$ species (i.e. 880 cm^{-1}) appears as a positive peak as it desorbs from the surface and an increased adsorption of a deprotonated species is observed at 800 cm^{-1}. An increase in the adsorbed carbonate species is also observed at 1450 cm^{-1} due to the pH increase in open air.

The titration experiments gave some indication of the behaviour of adsorbed As(III) and As(V) species on Fh. Although, there were experimental limitations with the titration experiments which included having to perform them at atmospheric conditions. Additionally the ionic strength was also increased as the pH was increased. Ideally, to determine the effects of increases in pH caused by the reduction of water during the application of reductive potentials, an *in-situ* pH measurement is required. Commercial pH electrodes were not viable for these experiments due to size constraints of the

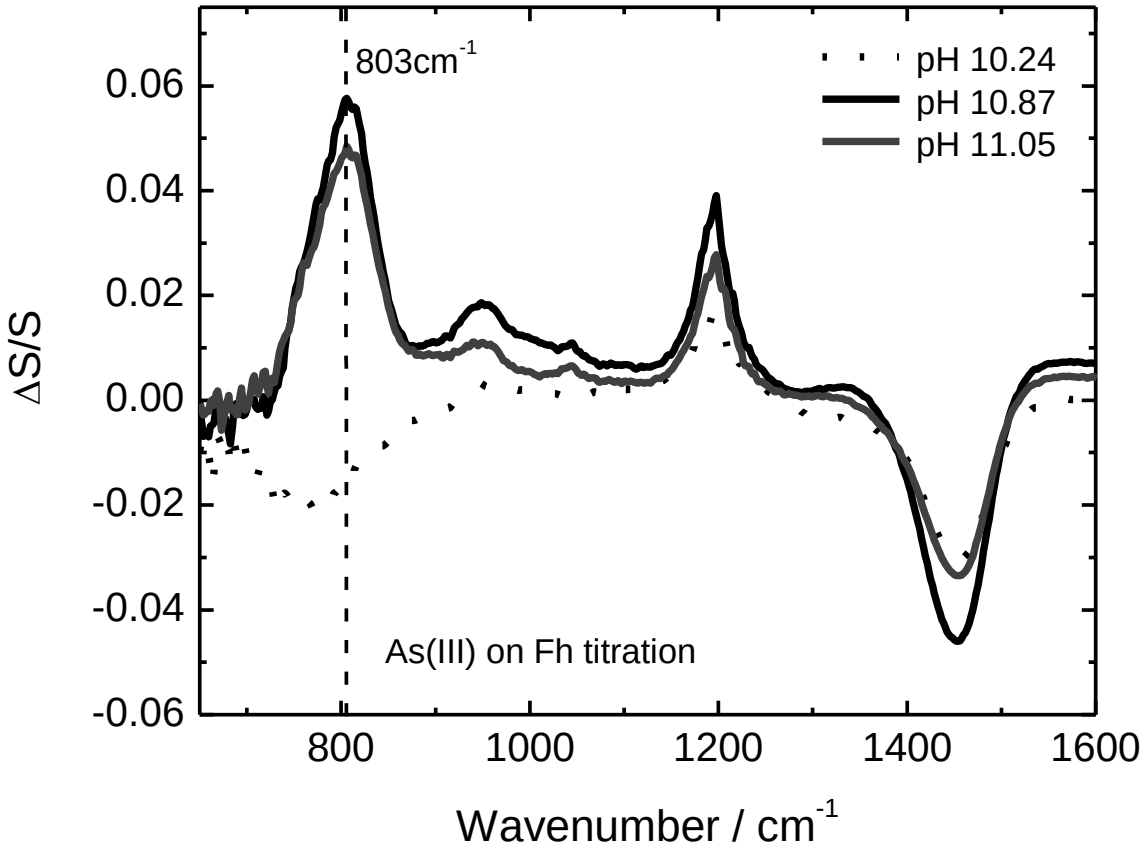

Figure 3- 13: Manual pH increase to As(III) adsorbed on Fh with 0.011 M NaOD solution at atmospheric conditions. Reference spectrum: 10 mM As(III) on Fh at natural pH ~10; Sample spectrum: after adjusting the pH.

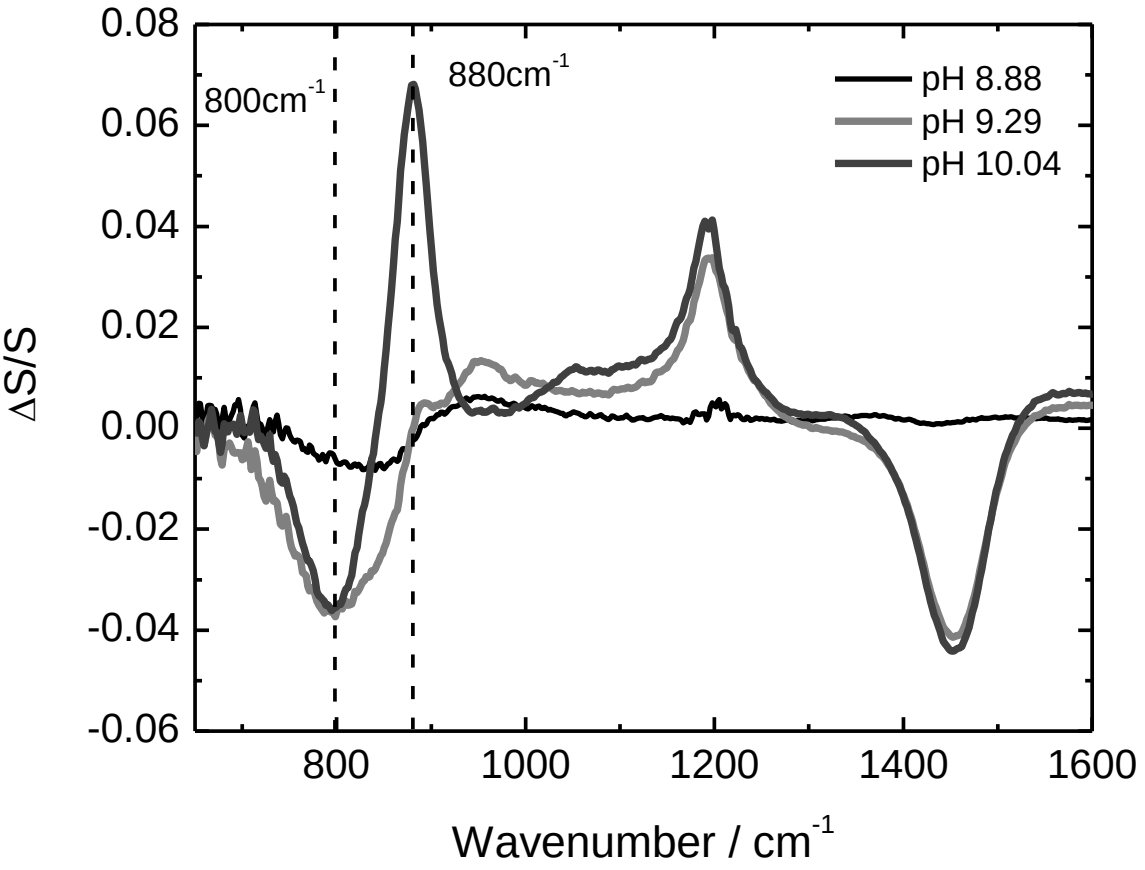

Figure 3- 14: Manual pH increase to As(V) adsorbed on Fh with 0.011 M NaOD solution. Reference spectrum: 10 mM As(V) on Fh at natural pH ~8.5; Sample spectrum: after adjustment of pH.

experimental setup. Upon investigation of the literature the most viable option was to fabricate an in-house pH sensitive probe. Several studies were found to have used palladium oxide wire for pH measurements; this was determined to be a feasible option for these experiments due to the relatively simplistic preparation.[29-37]

3.3.2. Palladium/Palladium Oxides pH measurements

The development of a Pd/PdO pH electrode was investigated in order to make *in-situ* pH measurements while applying negative potentials to the arsenic/ferrihydrite system. Several types of PdO preparation have been employed by previous researchers including electrochemical and thermal treatment. Based on literature findings, thermal formation of PdO provides better response then electrochemical formation.[33] For this reason thermal treatment methods were used in this study. As reviewed in the Introduction, the ideal response from a PdO pH electrode is a slope of -59mV/pH. Ideally a large change in potential measurement with changing pH is desired, as this would represent the analytical sensitivity of the measurement. In order to achieve this, several different wire preparations were established. Procedures of the thermal treatment and the insulation preparation are discussed in detail in the Experimental section.

The preparation of one wire was used to determine the feasibility of this type of measurement. The initial response of this wire was promising, although it did not maintain an appropriate pH response over a significant enough time period. This warranted further investigation for the formation of a PdO pH sensor. With limited calibration of this wire the response is shown in Figure 3-15a, with an average slope of -29 mV/pH ± 20 mV/pH and a % error of 51. Heating cycles for a second generation of Pd wires were completed in an oxygen swept furnace in order to obtain a better pH response, as reported by Grubb and King.[29] This resulted in significant improvement in the pH response, giving an average slope of -47 mV/pH although limited reproducibility with a standard deviation of 20 mV/pH was measured. The improvement between these two methods of preparation most likely has two contributions. First, a more

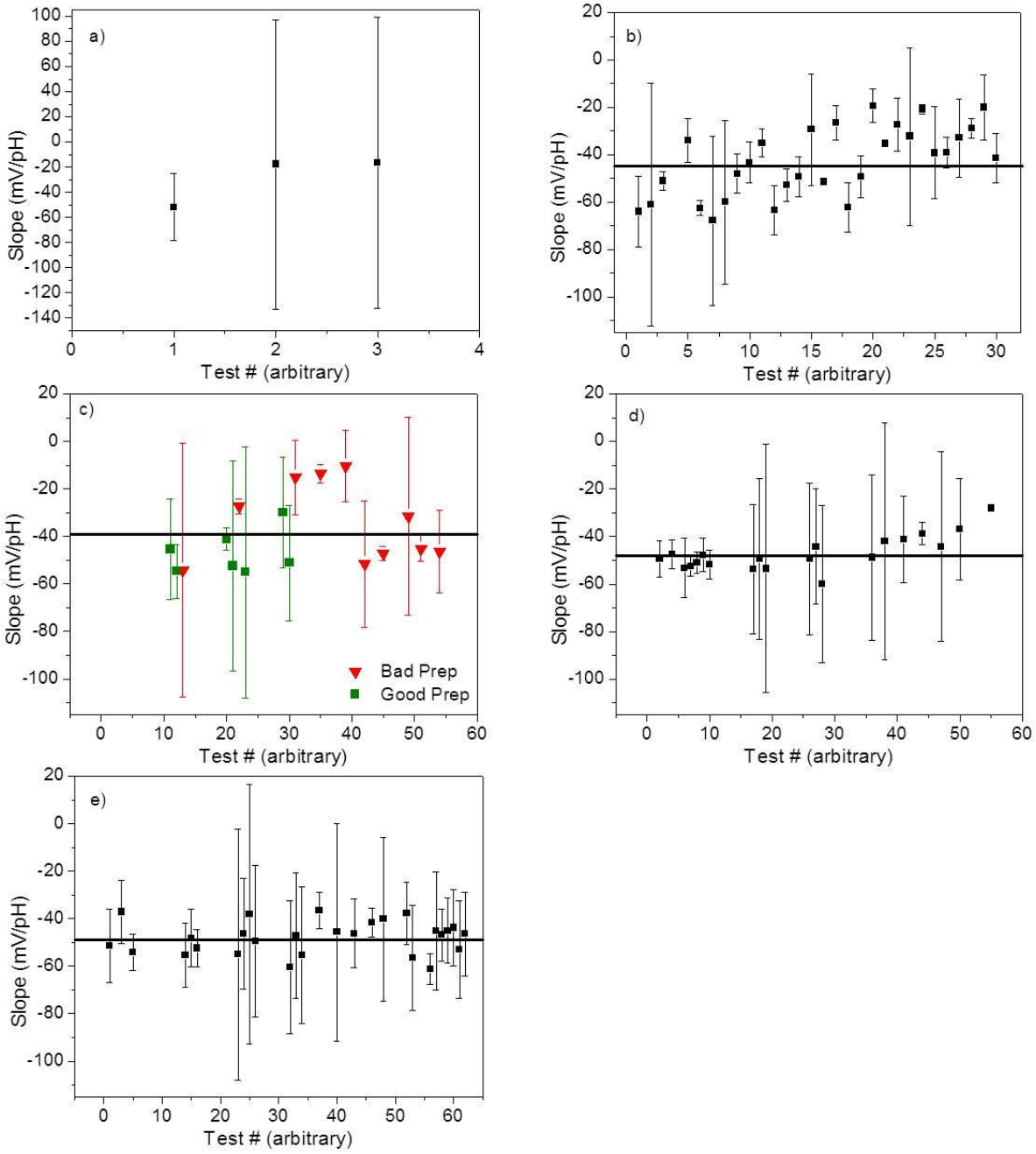

Figure 3- 15 a: First generation PdO preparation heating at 750°C for 20 minutes in air.

b: Second generation PdO preparation, heating at 750°C for 20 minutes with O_2 flow.

c: Third generation PdO preparation heated at 750°C 40 minutes with O_2 flow, comparison of good (■) and bad (▼) preparation.

d: Third generation PdO predation heated at 750°C 20 minutes O_2 flow.

e: Third generation PdO predation heated at 800°C 20 minutes with O_2 flow.

uniform oxide layer due to the oxygen swept furnace, and second the use of a sealant to ensure only the palladium oxide is exposed to solution and not the portion of the unoxidized wire.[29] A third generation of wires were prepared using three different temperature profiles along with optimal insulation of the wires to determine which obtained a better pH response (see Experimental chapter for details of the temperature profiles and insulation methods). Based on literature, proper insulation of the non-oxidized portion of the wire is important in the pH response of the electrode.[29,30,37] The three temperature profiles used were: 750°C for 20 minutes, 750°C for 40 minutes, and 800°C for 20 minutes, all with a flow of oxygen during heating and each profile was completed in triplicate. The wires heated at 750°C for 40 minutes are split into two different criteria, good insulation and bad insulation. This refers to how close the insulation was to perfectly sealing at the junction where the PdO meets the metallic Pd. The wire which was not insulated properly had approximately 1 mm of exposed oxide (compared to 3 mm on other wires). Also the epoxy used to seal the insulation to the wire coated most of the remaining exposed oxide, leaving only a small amount of PdO exposed. The wire which had bad insulation had a mean slope of -34 mV/pH with a standard deviation of 17 mV/pH compared to the better pH response from the good insulated wires with a slope mean of -47 mV/pH and standard deviation of 9 mV/pH. The ability to properly insulate the wires is shown in a greater response to changing pH, along with a considerable improvement in the reproducibility of the calibration. This is also a substantial improvement in the percent error between the poorly insulated wire at 42 % and the wires that had a better insulation at 20 %. The wires heated at 750°C and 800°C for 20 minutes gave very similar results with mean slopes of -47 and -48 mV/pH and the same standard deviation of 7 mV/pH, along with a slight change in % error with 20 % and 19 % (see Figures 3-15d and 3-15e). Overall, the wires prepared at these three temperature profiles performed equally well when insulated properly, a slight increase in the repeatability of the wires heated for 40 minutes at 750°C was the greatest difference between these wires. The successful calibration of these PdO pH sensors allowed for *in-situ* pH measurements with potential control to give an indication of the potential induced pH changes. Additionally, a Pt wire was placed in a similar configuration in order to make *in-situ* Eh measurements.

Although the pH response of the PdO wires was adequate for sensing changes in pH it was observed that there was a substantial change in potential value at a particular pH. Similar results were determined from Grubb and King, although to a lesser extent.[29] They attribute these differences to inconsistencies in the oxide layer. Presumably any inconsistency in the oxide layer would remain constant for each individual wire, thus this change should be limited while comparing individual wires. These changes are highlighted in Figure 3-16. Each calibration curve has a similar slope, between -46 and -48 mV/pH, although they have substantially different intercepts; changing by about 100 mV between the four curves. To adequately deal with this a final calibration curve was put together prior to performing pH measurements during potential application. The slope of this curve, -50 mV/pH, was used to determine major changes in the pH during the application of reductive potentials. This was performed by measuring the pH at the beginning of the experiment (with a pH meter) to correspond to the measured PdO potential at the same pH (Figure 3-17). During the application of reductive potentials the PdO potential was monitored and later converted to a pH using the slope of the calibration curve, -50 mV/pH (Figure 3-17).

3.3.3. pH and Eh measured changes due to potential application

Previous experiments determined that the PdO electrode is capable of adequately measuring pH changes in aqueous solutions. The PdO electrode used in potential control experiments was prepared at 800°C for 20 minutes and was securely fastened in the Au plated working electrode for measurement during application of reductive potentials. New measurements were made with this configuration to make a calibration curve used for pH determination during potential control, see Figure 3-17. An indication of the pH changes during potential application are given by the slope from this calibration curve, -50 mV/pH, and the starting measured pH. The changing solution potential, Eh, due to potential application is also given using a Pt (vs SCE) electrode setup in a similar fashion as the PdO pH sensor (see Experimental section of details on the configuration).

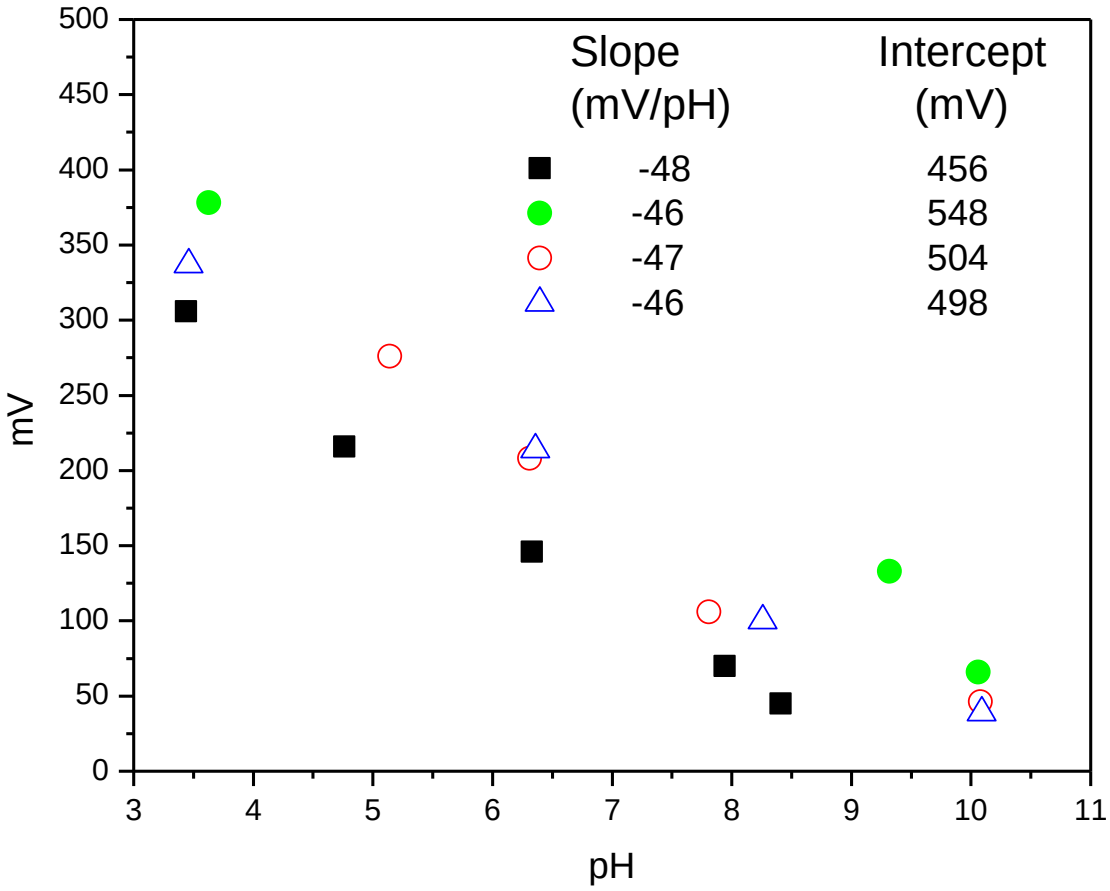

Figure 3- 16: Comparison of changes in intercept of PdO calibration curves while the slope remains relatively constant.

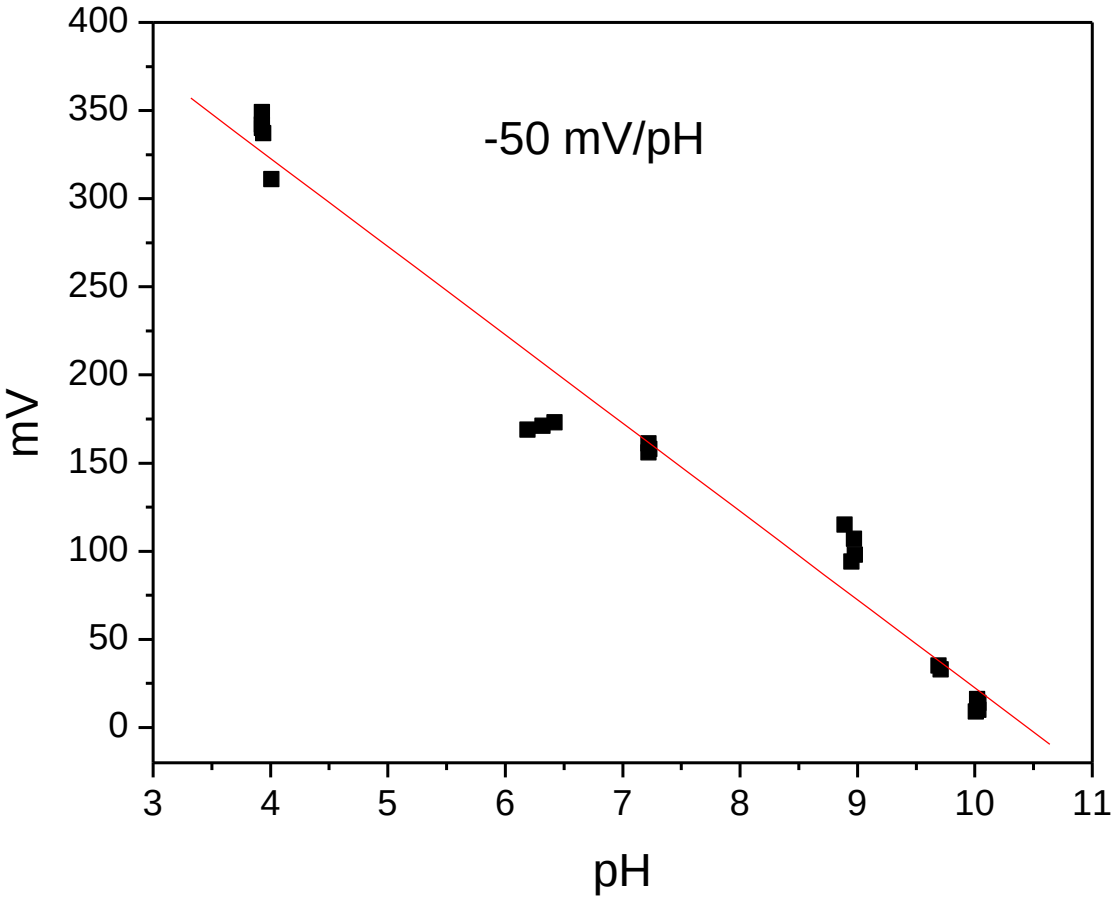

Figure 3- 17: Calibration curve for pH determination during potential control experiments

The results from these experiments are provided in Table 3-1. The initial experiment performed was on Fh alone in the absence of arsenic to indicate the changes in pH. The initial pH was 6.61 and with an application of -1000 mV the pH is substantially increased, to ~10. The initial pH of As(III) in solution is naturally high at 10.23, and is not substantially changed with the application of reductive potentials. The potential of the PdO electrode only changes by ~10 mV indicating only slight increases in the pH. Experiments performed with As(V) in solution had more significant changes. The initial pH was measured at 8.84 and during the application of -500 mV and -1000 mV was increased to 9.1 and 10.8. A substantial decrease in Eh to -358 mV (vs SCE) during -1000 mV application was observed. Using a Pourbaix diagram (Figure 3-18) the dominant As species in the thin volume of solution can be determined (note the solution potentials must be converted to NHE for comparison on the Pourbaix diagram). The dominant species in solution at pH 10.8 and Eh of -146 mV (vs NHE) is $As(OH)O_3^{2-}$. Drastic changes are observed at more negative potentials. With the application of -1200 mV the pH is substantially increased to ~12 and the Eh to -433 mV (vs SCE; -192 vs NHE), approaching conditions which favour a totally deprotonated AsO_4^{3-} species. This result agrees with the band assignments of AsO_4^{3-} appearing at 803 cm^{-1} from the ATR-FTIR spectroelectrochemical experiments (Figure 3-11). Presumably the generation of a totally deprotonated As(V) species is due to the drastic increase in pH and a decreased Eh at very high reductive potentials. The use of the PdO pH sensor during potential application gives an indication of the extensive increases in pH during these experiments.

The ATR-FTIR experimental setup allowed for differentiation of Fh adsorbed As(III) and As(V) at OCP. The successful design and development of a spectroelectrochemical cell allowed for *in-situ* IR measurements during electrochemical experiments. Spectroelectrochemical experiments associated applied reductive potentials to increases in pH due to the reduction of water to generate OH^-. In the absence of arsenic, Fh was found to release adsorbed sulfate and carbonate from the surface and at increased reductive potentials (-1200 mV) the dissolution of Fh. With the adsorption of As(III) to the Fh surface, spectroelectrochemical experiments measured the release of $As(OH)_2O^-$ species from the surface

Table 3- 1: Monitoring pH and Eh changes with applied potential. Initial pH is measured while the pH at any particular potential is determined from calibration curve (Figure 3-16), -50 mV/pH

Applied Potential mV (vs Ag/AgCl)	PdO mV (vs SCE)	pH	Eh mV (vs SCE)	Eh mV (vs NHE)	Dominant As Species in thin solution layer
5 mM SO_4^{2-} in solution					
Initial Conditions	203	6.61			---
-500	236	5.9	147	388	---
-1000	46	10.3	-422	-181	---
5 mM SO_4^{2-} and 10 mM As(III) in solution					
Initial Conditions	-159	10.23			
-500	-156	10.3	-49	250	
-1000	-166	10.4	-74	167	
-1200	-170	10.4	-216	25	
5 mM SO_4^{2-} and 10 mM As(V) in solution					
Initial Conditions	99	8.84			
-500	88	9.1	146	387	$As(OH)O_3^{2-}$
-1000	2	10.8	-358	-146	$As(OH)O_3^{2-}$
Initial Conditions	40	8.84			
-1200	-134	12.3	-433	-192	AsO_4^{3-}

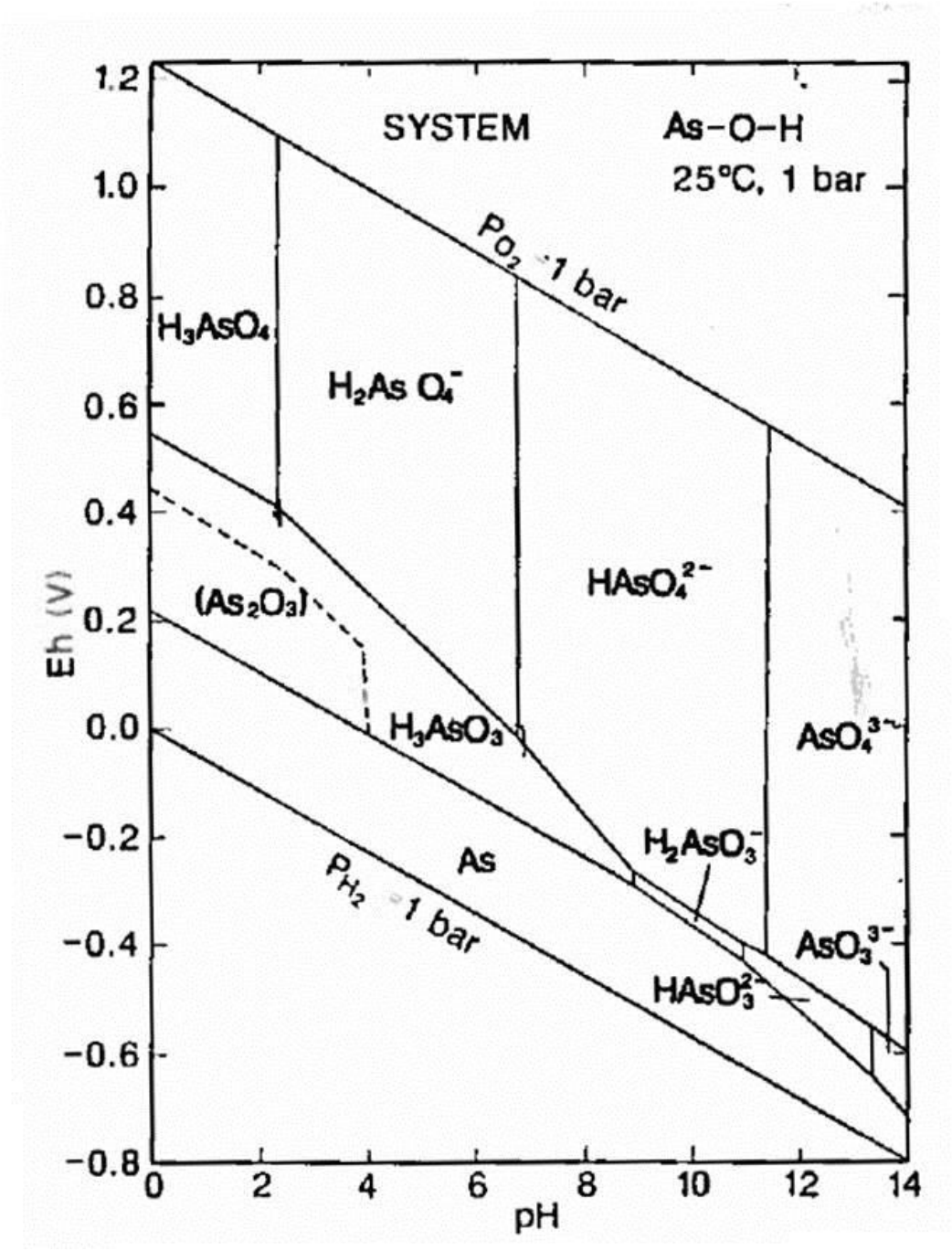

Figure 3- 18: Arsenic Pourbaix Diagram adapted from Brookings.[38]

of the Fh below -900 mV of applied potential. Arsenate was also observed to release from the surface of Fh at increasingly reductive conditions through successive steps of deprotonation. Arsenate at a natural pH of 8.5 is present as $As(OH)O_3^{2-}$ and at potentials ~-1200 mV the totally deprotonated species was found to be generated. Presumably the desorption of both As(III) and As(V) was due to electrochemical induced pH increases caused by the generation of OH^- during the reduction of water. To measure the changing pH a miniature pH sensitive probe was fabricated using Pd/PdO wire. *In-situ* pH and Eh measurements were made during electrochemical experiments by placing the PdO pH probe in the Au plated Ni WE along with an additional Pt electrode used for measurement of Eh. Increasing pH was successfully measured during potential application. In the presence of As(III) only a slight increase in pH was observed from the natural pH of 10. The pH was substantially increased in experiments containing As(V) and the increased pH and decreasing Eh measurements supported the generation of a totally deprotonated species, AsO_4^{3-}. This observation reinforced the appearance of an AsO_4^{3-} vibrational band in the spectroelectrochemical experiments.

3.4. Reference List

1. Müller, K.; Ciminelli, V. S. T.; Dantas, M. S. S.; Willscher, S. *Water Res.* **2010,** *44*, 5660-5672.
2. Goldberg, S.; Johnston, C. T. *J. Colloid Interface Sci.* **2001,** *234*, 204-216.
3. Tossell, J. A. *Geochim. Cosmochim. Acta* **1997,** *61* (8), 1613-1623.
4. Bargar, J. R.; Kubicki, J. D.; Reimeyer, R.; Davis, J. A. *Geochim. Cosmochim. Acta* **2005,** *69* (6), 1527-1542.
5. Carabante, I.; Grahn, M.; Holmgren, A.; Kumpiene, J.; Hedlund, J. *Colloids Surf. , B* **2009,** *346*, 106-113.
6. Parfitt, R. L.; Smart, R. St. C. *Soil Sci. Soc. Am. J.* **1978,** *42*, 48-50.
7. Parfitt, R. L.; Smart, R. St. C. *J. Chem. Soc. , Faraday Trans.* **1977,** *73* (1), 796-802.
8. Hug, S. J. *J. Colloid Interface Sci.* **1997,** *188*, 415-422.
9. Peak, D.; Ford, R. G.; Sparks, D. L. *J. Colloid Interface Sci.* **1999,** *218*, 289-299.
10. Su, C.; Suarez, D. L. *Clays Clay Miner.* **1997,** *45* (6), 814-825.
11. Brechbühl, Y.; Christl, I.; Elzinga, E. J.; Kretzschmar, R. *J. Colloid Interface Sci.* **2012,** *377*, 313-321.
12. Myneni, S. C. B.; Traina, S. J.; Waychunas, G. A.; Logan, T. J. *Geochim. Cosmochim. Acta* **1998,** *62* (19/20), 3285-3300.
13. Voegelin, A.; Hug, S. J. *Environ. Sci. Technol.* **2003,** *37* (5), 972-978.
14. Mazzetti, L.; Thistlethwaite, P. J. *J. Raman Spectrosc.* **2002,** *33*, 104-111.
15. Das, S.; Hendry, M. J.; Essilfie-Dughan, J. *Environ. Sci. Technol.* **2011,** *45*, 268-275.
16. Tufano, K. J.; Reyes, C.; Saltikov, C. W.; Fendorf, S. *Environ. Sci. Technol.* **2008,** *42*, 8283-8289.
17. Tufano, K. J.; Fendorf, S. *Environ. Sci. Technol.* **2008,** *42* (13), 4777-4783.
18. Coupez, J. *Anal. Chim. Acta* **1957,** *16*, 582-591.

19. Ursúa, A.; Marroyo, L.; Gubía, E.; Gandía, L. M.; Diéguez, P. M.; Sanchis, P. *Int. J. Hydrogen Energy* **2009,** *34*, 3221-3233.

20. Ulleberg, Ø. *Int. J. Hydrogen Energy* **2003,** *28*, 21-33.

21. Mazloomi, K.; Sulaiman, N. b.; Moayedi, H. *Int. J. Electrochem. Sci.* **2012,** *7*, 3314-3326.

22. Raven, K. P.; Jain, A.; Loeppert, R. H. *Environ. Sci. Technol.* **1998,** *32*, 344-349.

23. Dixit, S.; Hering, J. G. *Environ. Sci. Technol.* **2003,** *37*, 4182-4189.

24. Jessen, S.; Larsen, F.; Koch, C. B.; Arvin, E. *Environ. Sci. Technol.* **2005,** *39*, 8054-8051.

25. Langner, H. W.; Inskeep, W. P. *Environ. Sci. Technol.* **2000,** *34*, 3131-3136.

26. Burgess, I. J.; Seivewright, B.; Lennox, R. B. *Langmuir* **2006,** *22*, 4420-4428.

27. Masscheleyn, P. H.; Delaune, R. D.; Patrick, W. H. *Environ. Sci. Technol.* **1991,** *25*, 1414-1419.

28. Bhatti, N. K.; Subhani, M. S.; Khan, A. Y. *Tuk J. Chem* **2005,** *29*, 659-668.

29. Grubb, W. T.; King, L. H. *Anal. Chem.* **1980,** *52* (2), 270-273.

30. Kim, J. Y.; Lee, Y. H. *Biotechnol. Bioeng.* **1989,** *34*, 131-136.

31. Hu, C.-C.; Wen, T.-C. *Electrochim. Acta* **1996,** *41* (9), 1505-1514.

32. Lui, C.-C.; Bocchicchio, B. C.; Overmyer, P. A.; Neuman, M. R. *Science* **1980,** *207* (11), 188-189.

33. Kinoshita, E.; Ingman, F.; Edwall, G.; Glab, S. *Electrochim. Acta* **1986,** *31* (1), 29-38.

34. Macfie, G.; Cooper, A.; Cardosi, M. F. *Electrochim. Acta* **2011,** *56*, 8394-8402.

35. Horkans, J. *J. Electroanal. Chem.* **1986,** *209*, 371-376.

36. Stanic, Z.; Dimic, T.; Simic, Z. *J. Electrochem. Soc* **2012,** *159* (5), J168-J175.

37. Bloor, L. J.; Malcolme-Lawes, D. J. *Electroanal. Chem.* **1990,** *278*, 161-173.

38. Brookings, D. G. *Eh-pH Diagrams for Geochemistry;* Springer-Verlag: New York, 1988.

4. Conclusions and Future Work

4.1. Conclusions

The importance of understanding the behaviour of arsenic species in the environment is vital due to its toxicity. The sequestration of arsenic by iron(III) (oxy)hydroxides has been investigated by many researchers to obtain a greater understanding of its behaviour and what leads to its mobility.[1-6] Due to its natural occurrence in TMF at uranium mining facilities, ferrihydrite surrounds many of these studies. As Fh is metastable many investigations look to understand the fate of arsenic during phase transformations. Many of the current methods to investigate adsorption and desorption properties of arsenic on Fh introduce competing factors.[7-14] The focus of this thesis was to develop a method using electrochemistry to adjust conditions and determine the fate of adsorbed As species.

In order to successfully perform the required experiments a method needed to be developed in order to make the required measurements. A spectroelectrochemical cell was designed and machined (machining was done at the Physics Machine Shop) and successfully implemented for experiments. The specifications that the cell required were that it needed to seal on the surface of the IRE while still having enough surface area exposed to perform the electrochemical experiments. The cell also needed to accommodate the required electrodes and purging ports, which was accomplished. The initial design of the WE, which used a sputtered thin gold layer on the IRE, proved to be unsuccessful for the experiments because the gold surface was too reflective. The second design of the WE proved to be a success, which used a Au plated Ni bar that was placed on the surface of the Fh coated IRE for potential control.

ATR-FITR experiments were initially performed at open circuit conditions to determine the behaviour of As(III) and As(V) on Fh in addition to a method for characterization of Fh. The majority of the experiments were performed with ZnSe IRE which has a low wavenumber cut-off below 700 cm^{-1}.

The characteristic vibrational band for Fe-O is observed at ~700 cm^{-1} which allowed for its identification. ATR-FTIR was capable of differentiating between adsorbed As(III) and As(V) species. As(III) is present as a partially deprotonated species, $As(OH)_2O^-$ at natural pH of 10 which has a characteristic As-O vibration at 803 cm^{-1}.[15] While adsorbed, As(V) has an observed vibrational band centered at 836 cm^{-1}.[15] Upon deconvolution of the As(V) band it is found that there are two contributions to this feature. A lower wavenumber feature is at 803 cm^{-1} and is assigned to the As-OFe vibration while the feature at 847 cm^{-1} is indicative of the non-coordinate As-O of the same complex.[15] After understanding the adsorption behaviour of As(III) and As(V) on Fh the spectroelectrochemical experiments were performed.

An initial electrochemical experiment was performed to determine the fate of Fh with applied potentials using cyclic voltammetry. This experiment determined that reduction of Fe^{3+} to Fe^{2+} occurs below -600 mV applied potentials. During the spectroelectrochemical experiments it was expected that the dissolution of Fh should occur at approximately -600 mV. Initial spectroelectrochemical experiments were performed in the absence of adsorbed As species. These experiments used applied potentials of -400 mV and -500 mV which indicated little to no changes in the ATR spectra. With application of -700 mV and -1200 mV it was observed that sulfate and carbonate desorb from Fh in addition to its dissolution. As stated from the electrochemical experiment this result was expected at potentials below -600 mV. Spectroelectrochemical experiments performed on As(III) adsorbed on Fh observed a loss of the As(III) species from the surface as the major contribution. While the dissolution of Fh was not observed to a great extent, this was expected since adsorbed species tend to increase the stability of Fh. Spectroelectrochemistry of As(V) on Fh proved to be a more complicated endeavour. At potentials of -200 mV the generation of a $As(OH)_2O_2^-$ species is observed at ~900 cm^{-1}. This is most likely due to electric field induced pH changes. This species is then desorbed form the surface upon application of -800 mV. At applied potentials of -1200 mV the generation of a totally deprotonated species, AsO_4^{3-}, is observed at 803 cm^{-1} along with the loss of the adsorbed $As(OH)O_3^{2-}$ species at ~840 cm^{-1}. Since the potentials required to observe changes in the adsorbed As(III) and As(V) are quite negative it is most

likely that the changes that are occurring are due to the generation of OH^- during the electroreduction of water.

Concurrently, an experimental method to make *in-situ* pH measurements was developed. Due to the size confinement of the experimental apparatus a miniature pH sensor was required. Investigation of the literature found that palladium oxide had suitable pH response and stability.[16-20] A pH sensor made from Pd wire was fabricated using a thermal treatment at 750°C in an oxygen swept furnace. This pH sensitive PdO wire was small enough that it was possible to place it in the WE with a tapped screw. This made it possible to perform *in-situ* pH measurements during the application of reductive potentials. Additionally, a Pt wire was place on the opposite side of the WE in order to make *in-situ* Eh measurements during potential application. As with the spectroelectrochemical experiments an initial experiment was performed on Fh alone. This experiment measured a substantial pH change during negative potential application and the thin cavity's basicity was measured to increase by 4 pH units. The Eh change was measured to be +388 mV (vs NHE) at -500 mV applied and -181 mV (vs NHE) at -1000 mV applied. In the presence of As(III) on Fh the pH changes were not as drastic, only changing a fraction of a pH unit from 10.2 prior the potential application to 10.4 at -1200 mV applied potential. However, during this experiment the Eh changed by several hundred millivolts from 250 mV at -500 mV WE potential to 25 mV at -1200 mV WE potential. As with the spectroelectrochemical experiments the most drastic changes occurred with As(V) on Fh. The natural pH was measured at 8.8 which increased to 12.3 with the application of -1200 mV to the WE. In addition to the substantial reduction of the Eh from 387 mV (vs NHE) at applied -500 mV to -192 mV (vs NHE) at -1200 mV applied potential. Using the arsenic Pourbaix diagram and the pH and Eh measurements at -1200 mV WE potential the dominant species in solution is determined to be totally deprotonated, AsO_4^{3-}. This result confirmed the assignment for the ATR-FTIR band observed to increase at 803 cm^{-1} during the application of -1200 mV in the spectroelectrochemical experiment for As(V) adsorbed on Fh.

4.2. Future Work

Due to the low wavenumber cut-off the ZnSe IRE used in the spectroelectrochemical experiments it is not possible to determine the phase transformations of Fh with potential application. It would be beneficial to understand which iron(III) (oxy)hydroxides are being formed during application of reductive potentials. The most common phase transformations of Fh are the formation of α-Fe_2O_3 and α-FeOOH. The high intensity bands for these phases are below 700 cm^{-1} making them unobservable in the current ATR-spectroelectrochemical cell. The characteristic bands for hematite are located at 222 and 290 cm^{-1}, while for goethite the bands are located at 297 and 384 cm^{-1}.[21] For this reason Raman is required for the identification of these mineral phases. The development of a similar experimental method for use with Raman spectroscopy would be beneficial in understanding the effect of reductive conditions on Fh. Future work in this area of study would benefit from understanding the fate of Fh under reductive conditions.

It is important to obtain a greater understanding of the relationship between Eh and pH and the mobility of arsenic in TMFs. Having this understanding will potentially allow for long term determination of the fate of arsenic in TMF and ecological systems. This information could allow for an understanding of when the conditions in the TMF approach a situation where the release of As might become an issue. Potentially this would be done by interpretation of the conditions to determine if they favour the release of arsenate or arsenite from Fh or the transformation of Fh to a more stable iron(III) (oxy)hydroxide. This information would be most suitable for long term monitoring of the tailings system as in the short term the system is relatively stable. However, the implementation and/or the use of the results of this work would be somewhat complicated for several reasons. Firstly, considerable work would be required to be able to make pH and Eh measurements that accurately represent the conditions of the TMF. In addition, an approach to accommodating changing system conditions that could lead to a

possible release of As from Fh would have to be developed. Presumably with additional resources these complications can be overcome in order to properly understand arsenic sequestration and lability in the complicated geochemical matrices inherent to TMFs. It is hoped that the contents of this thesis will provide a starting point from which advanced understanding will aid in the ability to continually maintain the TMFs into the future.

4.3.Reference List

1. Moldovan, B. J.; Hendry, M. J.; Harrington, G. A. *Appl. Geochem.* **2008,** *23*, 1437-1450.
2. Shaw, S. A.; Hendry, M. J.; Essilfie-Dughan, J.; Kotzer, T.; Wallschläger, D. *Appl. Geochem.* **2011,** *26*, 2044-2056.
3. Ferguson, J. F.; Gavis, J. *Water Res.* **1972,** *6*, 1259.
4. Raven, K. P.; Jain, A.; Loeppert, R. H. *Environ. Sci. Technol.* **1998,** *32*, 344-349.
5. Jain, A.; Raven, K. P.; Loeppert, R. H. *Environ. Sci. Technol.* **1999,** *33*, 1179-1184.
6. Das, S.; Hendry, M. J.; Essilfie-Dughan, J. *Environ. Sci. Technol.* **2011,** *45*, 268-275.
7. Jones, C. A.; Langner, H. W.; Anderson, K.; McDermott, T. R.; Inskeep, W. P. *Soil Sci. Soc. Am. J.* **2000,** *64*, 600-608.
8. Erbs, J. J.; Berquó, T. S.; Reinsch, B. C.; Lowry, G. V.; Banerjee, S. K.; Penn, R. L. *Geochim. Cosmochim. Acta* **2010,** *74*, 3382-3395.
9. Kneebone, P. E.; O'day, P. A.; Jones, N.; Hering, J. G. *Environ. Sci. Technol.* **2002,** *36*, 381-386.
10. Langner, H. W.; Inskeep, W. P. *Environ. Sci. Technol.* **2000,** *34*, 3131-3136.
11. Tufano, K. J.; Fendorf, S. *Environ. Sci. Technol.* **2008,** *42*, 4777-4783.
12. Tufano, K. J.; Reyes, C.; Saltikov, C. W.; Fendorf, S. *Environ. Sci. Technol.* **2008,** *42*, 8283-8289.
13. Deuel, L. E.; Swoboda, A. R. *Soil Sci. Soc. Proc.* **1972,** *36*, 276-278.
14. Masscheleyn, P. H.; Delaune, R. D.; Patrick, W. H. *Environ. Sci. Technol.* **1991,** *25*, 1414-1419.
15. Goldberg, S.; Johnston, C. T. *J. Colloid Interface Sci.* **2001,** *234*, 204-216.
16. Karagounis, V. A.; Liu, C. C.; Neuman, M. R.; Romankiw, L. T.; Leary, P. A.; Cuomo, J. J. *IEEE Trans. Biomed. Eng.* **1986,** *BME-33*, 113-116.
17. Liu, C.-C.; Bocchicchio, B. C.; Overmyer, P. A.; Neuman, M. R. *Science* **1980,** *207*, 188-189.
18. Kim, J. Y.; Lee, Y. H. *Biotechnol. Bioeng.* **1989,** *34*, 131-136.
19. Grubb, W. T.; King, L. H. *Anal. Chem.* **1980,** *52*, 270-273.
20. Kinoshita, E.; Ingman, F.; Edwall, G.; Glab, S. *Electrochim. Acta* **1986,** *31*, 29-38.
21. Das, S.; Hendry, M. J. *Chem. Geol.* **2011,** *290*, 101-108.